IUE DATA REDUCTION

XXI. The Parameterization of the Motion of the IUE Reseau Grids and Spectral Formats as a Function of Time and Temperature

Randall W. Thompson, Barry E. Turnrose

Astronomy Department

Computer Sciences Corporation

and

Ralph C. Bohlin

Laboratory for Astronomy and Solar Physics

Goddard Space Flight Center

Submitted for publication in Astron. and Astrophys.

SUMMARY

Variations of temperatures within the International Ultraviolet Explorer (IUE) cause shifts in the measured location of the fiducial reseau marks and in the location of the spectral format with respect to the reseau grid. Correlations of the systematic behavior of these motions as a function of time and of the camera head amplifier temperature (THDA) have been found for the Long Wavelength Redundant (LWR) and Short Wavelength Prime (SWP) cameras.

Motion of the apparent location of the reseaux within a digitized image is found to be independent of time for both cameras. In the case of the LWR camera, the reseau locations are also nearly independent of THDA, but do show a stability of typically < 0.3 pixel without correction. In the case of SWP, a decrease in THDA correlates with an overall non-uniform expansion of the observed reseau positions. Shifts as large as 1.5 pixels are observed for a change in THDA of 9C, but this motion can be predicted using THDA to an accuracy of < 0.2 pixel. Since the SWP reseau motion is the most pronounced in the region of the camera where the high dispersion orders crowd together, the reseau temperature correction helps in locating the minimum background signal, which is precisely centered between the echelle orders.

Thermal changes alone do not account for all of the observed spectral format motion; in addition, secular variation is present. Models describing the motion of the high dispersion spectral format as a function of THDA alone reduce the scatter in the predicted position of a given wavelength; however, the scatter can be further reduced if a linear dependence on time as well as THDA is allowed. A correction technique is presented for early data, where errors that are sometimes over 30 km s^{-1} can be reduced by more than a factor of 10.

The primary benefit to the user of IUE data is a precision in wavelength that is now comparable to the wavelength accuracy of UV spectra obtained by the Copernicus satellite. Except for images where the IUE is at a temperature extreme not covered by the present data set, the corrections for time and temperature should result in a typical 1σ uncertainty of only 2.0 km s^{-1} for SWP and 2.7 km s^{-1} for LWR in the assigned high dispersion wavelength scales for targets centered in a large or small aperture. Spacecraft pointing errors, particularly in the case of blind offsets, may cause a different type of error that is due to de-centering of the target in an aperture. Besides the errors in assigning wavelengths to IUE spectra, there is additional uncertainty introduced in locating the centroids of features in extracted spectra which depends on the number and quality of the spectra analyzed; the amount of this independent error may be more or less than the above values of the intrinsic uncertainty.

I. INTRODUCTION

Historically at GSFC, the fiducial reseau positions that determine the geometric distortion of IUE images and the dispersion relations that track the spectral format have been updated at approximately biweekly intervals using standard WAVECAL images consisting of Pt-Ne emission spectra superposed on tungsten-flood (TFLOOD) backgrounds. Since July 1978 reseau positions have been measured exclusively on the low dispersion Pt-Ne-plus-TFLOOD images to avoid the occasional contamination of reseaux caused by the presence of a high dispersion Pt-Ne spectrum. Approximately sixty sets of reseau positions and dispersion constants have been accumulated for each camera and dispersion mode.

Although reseau positions and dispersion relations determined from the biweekly calibrations exhibit significant variation, this work is the first detailed study quantitatively relating the observed variations to temperatures and time. Preliminary results have been presented elsewhere (Thompson, Turnrose, and Bohlin, 1980 and Thompson, et al. 1980a). As an interim procedure, the use of mean reseau positions and mean dispersion relations in standard production processing was initiated in July 1980 at GSFC (Thompson, et al. 1980b). The use of mean calibration data eliminated the biweekly discontinuities in the way the IUE data were reduced. This paper describes the details of further improvements to IUE data reduction due to the correction of the mean reseau positions and dispersion constants for temperature variations and secular effects.

II. RESEAU MOVEMENT

A. Observed Motion

Independent of the spectral format, the measured positions of reseau marks on the IUE images are known to change from one image to the next due to a thermal sensitivity of the camera readout electronics (Oliver et al. 1979). In this analysis, the camera head amplifier temperature (THDA) at the time the image was read is chosen as the temperature measurement, because its value is available from the observing scripts for many images, from printed listings of hourly camera snapshots (maintained by the IUE operations control center) for many other images, and from the science header on Guest Observer tapes for images acquired since March 14, 1979, at GSFC and since May 16, 1979 at VILSPA. The two other thermistor temperatures currently recorded in the image header label were also studied for correlation with reseau motion. The digital-to-analog-converter thermistor (TDAC) showed little if any correlation with reseau motion. The other thermistor located in the camera deflection coil (TDC) showed correlations similar to those of THDA. However, TDC fluctuates during the camera prep-expose-read cycle, making critical the exact time of recording the temperature.

In analyzing the data on reseau positions, UVFLOOD flat-field exposures, rather than the standard set of low dispersion Pt-Ne-plus-TFLOOD exposures, are used, because complications in determining a few reseau positions can arise from the presence of the low dispersion Pt-Ne-spectra on the TFLOOD flat fields. Measurements of reseaux on some 15 LWR and 18 SWP 60% UVFLOOD images acquired over the first two years

of IUE operation are studied for temperature effects (see also Thompson et al. 1980b). Figure 1 summarizes some of the results of the temperature-dependence studies of reseaux conducted on in-flight images. This figure represents three separate sets of reseau measurements, each corresponding to a different THDA value. The diamond symbols indicate the positions of a low-temperature reseau set. From these positions, the displacements are drawn to the location of all corresponding reseaux from two higher-temperature images. Notice that reseau positions near the tube edge for SWP shift as much as $\sim$1.5 pixels with the change in THDA of 9 C between the diamonds and the highest temperature point.

B. Effects on Data

Because of the variations in measured reseau positions displayed in Figure 1, any particular biweekly calibration may be atypical if it corresponds to an extreme temperature. Figure 1 shows that reseau motion is largest in the upper right-hand portion of the SWP tube, where the high dispersion echelle orders are closest. Because of the differential, non-uniform nature of the reseau movement across the tube, the spectral registration step (see section III) cannot be equally effective at all portions of the tube; and since the closely spaced echelle orders at the short wavelengths are most susceptible to significant extraction errors, fluxes from SWP at short wavelengths have suffered the most from differential reseau motion. The improvement realized with the temperature correction technique over the use of mean calibration files is illustrated in Figure 2, where the corrected dispersion constants locate a lower background precisely between the spectral orders.

C. Modeling Results

Linear regressions for the reseau positions verses THDA were calculated separately in the line and sample directions for both the SWP and LWR cameras. No evidence was found for secular variation of reseau position. Figure 3 quantifies the linear correlation for the particular reseau mark near the upper center of the SWP tube in row 3 and column 7 of the 13 by 13 reseau grid, in the region of greatest observed motion. The maximum error in position for this reseau mark has been reduced from a possible extreme approaching 1.5 pixels using the old biweekly calibrations, to an amount $1\sigma < 0.2$ pixel using temperature corrections based on the linear THDA correlation. If all the reseaux within the target ring are considered, the average 1σ rms scatter in position can be reduced from 0.29 to 0.19 pixels in SWP and from 0.24 to 0.21 pixels in LWR by applying temperature corrections. The improvement for each individual reseau mark is displayed in Figures 4 (SWP) and 5 (LWR), which show the 1σ scatter before and after correction in the direction along and perpendicular to the high dispersion direction.

Another benefit from parameterizing the SWP reseau motion is a potential reduction in noise due to better alignment of the data image with the fine structure in the flat fields of the Intensity Transfer Function (ITF). However, initial results indicate that the improvement in global signal to noise is less than 5 percent, even for a SWP extreme of 14 C.

III. SPECTRAL FORMAT MOVEMENT

A. Observed Motion

The motion of IUE spectra with respect to the reseau grid has long been observed (Klinglesmith, Perry, and Turnrose, 1979). The standard

reduction procedures for a well-exposed continuum source routinely incorporate a spectral registration, which compensates for the component of spectral motion perpendicular to the dispersion direction. However, the component of spectral motion parallel to the dispersion direction cannot be removed in a similar and routine way at the time of processing. In order to solve this problem, the dispersion relations, which relate pixel location to wavelength and order number, have been evaluated to determine the movement of particular wavelengths within the image line and sample grid from one Pt-Ne wavelength calibration image to the next. Since the reseau positions used to geometrically correct the Pt-Ne (WAVECAL) images in this analysis are measured directly on the low dispersion Pt-Ne-plus-TFLOOD images, and since no high dispersion WAVECAL images are considered if they were obtained more than 3 hours earlier or later than the accompanying low dispersion image, none of the spectral shifts discussed here should be significantly contaminated by reseau motion.

The observed spectral shifts can be transformed for each camera and dispersion mode into orthogonal components parallel and perpendicular to the dispersion direction. Such a coordinate system is convenient, because the magnitude of the observed shift is revealed along the direction for which compensation is otherwise difficult to achieve. Figure 6 illustrates the observed shifts with respect to the mean along the dispersion direction for the high dispersion mode as a function of THDA. The shifts are smaller in the direction perpendicular to the dispersion and less important in the sense that they are compensated by the spectral registration step. In low dispersion, the shifts are similar; but

because the orders are orthogonal to the high dispersion orders, the greater shifts are in the direction perpendicular to the dispersion. In both high and low dispersion, the observed shifts are nearly constant in pixels within a given image.

B. Effects on Data

In the IUE high dispersion format, the dispersion varies both within a given echelle order and from one order to the next, but an increment of a pixel along an order corresponds to a wavelength increment $d\lambda$, which is very nearly proportional to the wavelength λ. Because of this, a given pixel shift, anywhere on the tube, corresponds very closely to a constant $d\lambda/\lambda$ and hence a constant velocity shift. For high dispersion, a shift of 1 pixel along any echelle order corresponds approximately to a velocity shift of 7.7 km s^{-1} for SWP and 7.3 km s^{-1} for LWR. As Figure 6 shows, the relative shift along the dispersion among the high dispersion WAVECAL images can be more than 4 pixels (30 km s^{-1}). The velocity-like wavelength errors in high dispersion reported by Leckrone (1980) are probably a direct consequence of this shifting of the spectral format.

In low dispersion, the shifts in the dispersion direction are only about half of the high dispersion motion and correspond to a constant wavelength shift per pixel (1.67 Å/pixel in SWP, 2.65 Å/pixel in LWR), rather than a constant velocity shift.

C. Modeling Results

THDA is the best available temperature parameter for describing spectral format motion, even though THDA is a camera temperature and only an indirect measure of thermal conditions within the spectrographs

themselves. The results of a linear fit to the observed motions are shown in Figure 6, where a change of 1 C in THDA corresponds to a mean motion of 0.30 pixel in SWP and 0.65 pixel in LWR. Encouraging as these correlations are, changes in THDA alone cannot fully parameterize the observed spectral motions. Figure 7 displays the spectral shifts along the orders after correcting with the linear regression relation of shift versus THDA only. The fact that the temperature correction has not removed all systematic effects is evidenced by the residual linear slope of about 0.7 pixel per year in the data in Figure 7. The observed motion for the component perpendicular to the high dispersion orders and for low dispersion are not illustrated but show a behavior similar to that illustrated in Figures 6 and 7.

Figure 7 indicates that a bivariate linear correlation of shift with both time and TDHA is required. After making this correction, the final column of Table 1 summarizes the average residual scatter (see below). The previous three columns summarize the scatter with no correction to the mean dispersion constants and with THDA corrections and time corrections only. Inspection of the numbers in Table 1 confirms our conclusion that corrections for both time and THDA are required to optimize the accuracy of predicted wavelength locations.

In order to compute the values in Table 1 the original dispersion constants for each WAVECAL are used to predict the location of the set of wavelengths corresponding to the IUE master Pt-Ne line libraries (Harvel, Turnrose, and Bohlin 1979 and Turnrose and Bohlin 1981). The mean dispersion relations are corrected as indicated in Table 1 and are then used to predict another set of positions for the same Pt-Ne line wavelengths. A 1σ rms residual scatter between the pairs of predictions

is computed at each wavelength, and then the average σ is found and presented in Table 1. The rms scatter in the two orthogonal directions for each emission line in the libraries is shown graphically in Figures 8 through 11 for the case of no correction and for the final best correction using time and THDA. In supplementing the mean dispersion constants with a time and temperature correction, the mean velocity error in high dispersion has been reduced from 4.4 to 2.0 km s^{-1} for SWP and from 8.5 to 2.7 km s^{-1} for LWR.

The fact that the amount of scatter varies across the tubes, particularly for SWP in high dispersion, is an unexpected result. The amount of scatter tends to increase toward the periphery of SWP. Reseau motion between the neighboring TFLOOD image used to define the reseau positions and the WAVECAL image used to determine the individual dispersion constants might be the problem. On the other hand, the cause might be a numerical instability in the regression analysis used to determine the individual sets of dispersion constants from the found line positions on each WAVECAL image. In the latter case, the dispersion constants might have too many degrees of freedom, so that noise in found line positions could induce spurious curvature in the polynomial fits. The fact that some of the less important coefficients in Table 6 differ significantly from the previously published means (Thompson et al. 1980b) supports the latter possibility.

IV. NUMERICAL RESULTS AND IMPLEMENTATION IN PRODUCTION PROCESSING

The corrections for thermal and temporal shifts were implemented as part of the standard data processing at GSFC on March 3, 1981 in low dispersion and on May 19, 1981 in high dispersion by a new applications

program called TCCAL. Using the time and THDA extracted from the IUE standard image header, the program generates the appropriately corrected reseau displacements and dispersion constants for each image processed. In order to help the users of IUE data understand the specifics of the reduction procedures, information has been added to 5 lines of the alphamuneric label appearing on the standard IUE tapes and plots. In the future, the procedures detailed here will be updated as necessary. The monitoring and continuing evaluation will utilize the flat field and WAVECAL images that are still acquired on a regular basis.

A. Reseau Displacements

The reseau displacements are the differences between the reseau positions found on a raw image and the actual 13 by 13 reseau grid located between the UV converter and the SEC vidicon camera. The mean displacements in Tables 2 (SWP) and 3 (LWR) describe the mean geometric distortions in the SEC vidicon detector and are the found minus the actual positions. The actual sample positions are the first row of integers at the top of Tables 2 and 3, while the actual line numbers are in the first column. The actual grid is on 56-pixel centers for SWP and 55 for LWR. The displacements at each actual reseau position in Tables 2 and 3 are in sample (upper entry) and in line (lower entry). The effective mean THDA is $\sim$9 C for SWP and $\sim$13 C for LWR.

Because the average scatter in the LWR reseau positions is reduced only from 0.24 to 0.21 pixel and because there are no large local deviations, the THDA correction is not applied in LWR production prosessing. For SWP, a greater global reduction in reseau scatter from 0.29 to 0.19

pixel , as well as even larger local improvements, are realized; therefore, the temperature corrections are in the standard SWP processing. If THDA at the time of read cannot be extracted from an image label, processing defaults to the mean reseau displacements.

The corrected SWP reseau displacements are equal to a value R(s) in sample and R(l) in line, such that

$$R = R_1 + R_2 T \tag{1}$$

where T is THDA and R_1 and R_2 are found in Tables 4 and 5 in the position corresponding to the same line or sample displacement of Table 2.

B. Dispersion Constants

The dispersion constants define the sample (s) and line (l) position of a given wavelength (λ in Å) and order (m). In high dispersion,

$$s = a_1 + a_2\, m\lambda + a_3\, (m\lambda)^2 + a_4\, m + a_5\, \lambda + a_6\, m^2\lambda + a_7\, m\lambda^2 \tag{2}$$

$$l = b_1 + b_2\, m\lambda + b_3\, (m\lambda)^2 + b_4\, m + b_5\, \lambda + b_6\, m^2\lambda + b_7\, m\lambda^2 \,. \tag{3}$$

Note the formulae (2) and (3) have the $m^2\lambda$ and $m\lambda^2$ coefficients improperly specified in the Nature article of Boggess et al. (1978). In low dispersion,

$$s = a_1 + a_2\lambda \tag{4}$$

$$l = b_1 + b_2\lambda. \tag{5}$$

The a and b coefficients above are found by a multivariable regression analysis of the found line positions and their wavelengths from the master line libraries.

The IUE program TCCAL computes the correction to the mean dispersion constants using the THDA temperature (T) at the end of the exposure and the date (t) defined as the number of days since January 1, 1978. If THDA is not available at the end of the exposure, the THDA at time of read is used.

The corrected dispersion constants are the means plus a value W, where W(s) and W(l) are the corrections to the appropriate equations 2 through 5.

$$W = W_1 + W_2T + W_3t \qquad (6)$$

The mean values of the a and b dispersion constants and the correction coefficients W are in Table 6 for the case of the IUE small aperture. The corrections to the dispersion relations have been implemented in terms of line and sample for operational simplicity, rather than in the transformed coordinates parallel and perpendicular to the dispersion as discussed in the previous section.

C. Changes to the Labels of the Data Products

A description of the temperature and time corrections are now included in the alphamuneric label. Specifically, in a line beginning "Mean Reseau", the time period used to define the mean reseau positions is identified by "GMT=", the number of flat field images used to define the correlations of motion with THDA is denoted "NO. FF=", and the 1σ scatter in sample and line are "SIGS=" and "SIGL=" in pixels "PX". The line beginning with "MEAN DC" contains similar time period and 1σ scatter information for the dispersion constants and "NO. WLC" means the number of WAVECAL images analyzed. Two more lines give the THDA values for the temperature corrections, with comments as appropriate. The line beginning "THERMAL SHIFTS:" contains W(l) and W(s) for the time and temperature corrections

to the dispersion constants. The old line "REGISTRATION SHIFTS:" remains as the final shift applied to register the dispersion constants with the spectrum by shifting perpendicular to the dispersion, but is now only the residual shift after the above "thermal shifts" are applied. Thus, the final dispersion constants used and listed in the header are the mean values for the particular large or small aperture, plus the "thermal" and "registration" shifts.

In addition to modifications to the label, more information is now included in numerical form in the data header record (also known as record zero and sometimes as the scale-factor record) of extracted spectral files on the standard IUE magnetic tapes. Specifically the following 16-bit words are:

Word	Contents
18	Sum of W(1) and registration shift in the line direction
19	Sum of W(s) and registration shift in the sample direction
20	THDA at the time of read
64	THDA at the time of the end of exposure

A value of zero for THDA means that no temperature corrections have been made to the mean reseau displacements or dispersion constants. Note, these changes to record zero are now in effect for the revised low dispersion software (Turnrose, Bohlin, and Lindler 1981) and will appear in high dispersion when that software package is revised for production.

V. COMPUTATION OF THE WAVELENGTH CORRECTION FOR ARBITRARY DISPERSION CONSTANTS

Although it is probably not practical to correct reseau positions ex post facto, the adjustments to the dispersion constants for time and temperature can be made for data reduced prior to the implementation of the corrections in production. Figures 12 to 15 show the predicted sample and line location for a given wavelength and order in the small aperture as a function of date and THDA. The mean position of the wavelength for the effective mean time and temperature is marked by a cross. Since the spectral format shifts as modeled are independent of position on the tube, the line and sample values that are assigned to the test wavelength and order using the dispersion constants specified in the image header of the original data reduction can be used to compute the wavelength correction as follows. The error is the vector from the point in the figure calculated from the original dispersion constants to the point predicted from the time and THDA of image acquisition. The error in wavelength is the projection of this vector onto the dispersion direction shown in the appropriate one of Figures 12 to 15. The sense of the correction is that, if the vector points in the same direction as the dispersion direction arrow, then the original wavelengths specified should be decreased. As explained in detail in the previous section, the magnitude of the correction should be converted using the plate scales in Table 6 for the appropriate camera and dispersion.

In the case of a large aperture spectrum, the same procedure as above can be applied after subtracting the offsets between the small aperture and the object position in the large aperture from the dispersion constants in the image header. The present standard offsets in pixels

are in sample and line -17.4 and -19.7 for SWP and -18.6 and +19.4 for LWR. See Turnrose, et al. 1979 for details and caveats for data obtained prior to August 1, 1979.

VI. OVERALL WAVELENGTH ACCURACY OF CORRECTED DATA

The final uncertainty in a measurement of a spectral feature in an IUE spectrum depends on both the accuracy to which the wavelengths are assigned and on the ability of the astronomer to determine the feature's centroid. This paper addresses the accuracy of the assigned wavelengths. Because we have averaged reseau positions and dispersion constants from independent measurements of many images, the error in our mean values should be negligible. Errors in the mean dispersion constants are further reduced by the polynomial smoothing of measured line positions in the normal reduction of each WAVECAL image. Thus, the wavelength accuracy of a typical astrophysical spectrum is given by the rms scatter parallel to the dispersion in the final column of Table 1, to the extent that the THDA is typical of the range considered here (see Figure 6). Figure 8 shows some evidence that the errors expected for SWP in high dispersion may be increased by $\sim$50% near the tube periphery.

To the extent that the residual reseau motion is not already included in the scatter of predicted wavelengths, the wavelength error expected will increase slightly. The worst case increase in high dispersion would be for a scatter of reseaux parallel to the LWR dispersion as large as 0.2 pixel at the edge of the tube. Even in this case, the 1σ error increases from 0.37 to only 0.42 pixels. Neglecting the small effects of residual reseau scatter, the conversion of the values in

Table 1 produces typical expected errors of 2.0 km s^{-1} (SWP, high), 2.7 km s^{-1} (LWR, high), 0.33 Å (SWP, low), and 0.64 Å (LWR, low).

Consider the following examples of the actual accuracy of measurements of narrow features in IUE high-dispersion SWP spectra. For an isolated narrow feature with the instrumental resolution of 2.5 pixels in the cleanest IUE data, the best possible estimate of the measurement accuracy would be $\sim$0.25 pixel. Combining this with the 0.26 pixel uncertainty in wavelength assignments in the center portion of SWP results in a net rms expected 1σ error of 2.8 km s^{-1}. Measuring N lines of the same velocity species in the same spectrum would reduce the 0.25 pixel error by the square root of N, but the original error of 2.0 km s^{-1} is probably systematic within a given specturm. On the other hand, measurements of the single line in N independent IUE spectra would reduce the total error of 2.8 km s^{-1} by the square root of N. In many cases, the data will not be of sufficient quality to approach a 0.25 pixel measurement error, so that the intrinsic errors in IUE wavelength scales are now often negligible in practice.

Errors for large aperture spectra should be the same as for the small aperture, since the procedure and accuracy of placing a target in the large aperture is the same as for the small aperture. An additional pointing error of 1" or 2" plus any uncertainty in the object coordinates must be considered when using the blind offset technique for crowded fields or very faint objects. A pointing error of 1" along the dispersion direction is 0.66 pixel or about 5 km s^{-1} in high dispersion. Even in the case of normal pointings, little information exists about errors on the order of 0".5. Perhaps, small aperture point sources could show

effects due to decentering in the 3" aperture by ± 0".5, whereas the Pt-Ne WAVECAL images cannot, because the 3" aperture is filled by the onboard light source.

In summary, errors in wavelength assignments of IUE data have been reduced from an extreme of over 30 km s^{-1} to less than 3 km s^{-1} in high dispersion. The residual uncertainty of 2 km s^{-1} for SWP and 2.7 km s^{-1} for LWR makes the wavelength accuracy of time and temperature corrected IUE spectra comparable to that of temperature corrected data from the Copernicus satellite.

Acknowledgements. We thank D. York for emphasizing the importance of absolute radial velocities for interstellar lines and D. Leckrone for discussions of the value of precise wavelength scales for stellar spectra. The operational side of the IUE Observatory staff at Goddard Space Flight Center continues to conscientiously collect a consistent body of wavelength calibration data.

Table 1

Error (1σ in Pixels) for Various Corrections

to the Mean Dispersion Constants

Dispersion Direction	No Correction	THDA Only	Time Only	THDA and Time
SWP high				
parallel	.58	.39	.39	.26
perpendicular	.27	.25	.23	.16
SWP low				
parallel	.38	.38	.25	.20
perpendicular	.55	.42	.37	.30
LWR high				
parallel	1.16	.54	.98	.37
perpendicular	.26	.22	.25	.21
LWR low				
parallel	.31	.26	.30	.24
perpendicular	1.13	.65	.81	.32

Table 2

Mean SWP Reseau Displacement Values

SAMPLE:	74	130	186	242	298	354	410	466	522	578	634	690	746
LINE 54	3.28	2.38	2.16	1.27	1.25	-.06	-2.46	-5.33	-8.89	-13.67	-17.09	-21.70	-25.37
	16.88	13.85	11.41	7.80	4.71	1.77	-.92	-3.05	-4.75	-5.02	-5.30	-4.18	-4.06
110	3.26	2.35	2.13	1.24	.82	-.19	-2.04	-4.37	-7.43	-12.21	-15.63	-20.24	-23.92
	14.74	11.72	9.28	5.66	2.58	-.23	-2.75	-4.80	-6.36	-6.63	-6.91	-5.79	-5.67
166	3.05	2.14	1.92	.95	.51	-.12	-1.62	-3.44	-5.99	-9.80	-13.22	-17.83	-21.50
	13.70	10.68	8.24	4.63	1.51	-1.13	-3.63	-5.75	-7.04	-7.58	-7.86	-6.74	-6.62
222	2.61	1.70	1.67	.93	.69	.16	-.85	-2.15	-4.40	-7.46	-10.56	-15.17	-18.84
	11.95	8.93	6.78	3.56	.93	-1.72	-3.92	-5.94	-7.10	-7.70	-7.91	-6.79	-6.66
272	3.78	1.73	1.77	.88	.84	.74	.13	-.58	-2.14	-4.73	-6.83	-11.09	-14.76
	9.38	7.31	5.66	2.91	.30	-2.19	-4.26	-6.12	-7.35	-7.91	-8.16	-7.13	-5.19
334	5.69	3.28	3.11	2.05	1.91	1.74	1.28	.80	-.54	-2.76	-4.84	-8.54	-12.21
	7.68	6.50	5.26	3.12	.90	-1.44	-3.59	-5.35	-6.81	-7.70	-7.86	-7.18	-5.24
390	7.15	4.82	4.28	3.04	2.83	2.84	2.58	2.21	1.51	-.27	-1.78	-5.20	-8.41
	6.74	5.86	4.85	3.19	1.15	-1.05	-3.09	-4.89	-6.33	-7.34	-7.70	-7.36	-5.93
446	10.56	7.35	6.42	4.96	4.33	4.18	4.08	3.77	2.94	1.51	.12	-2.66	-5.27
	5.71	5.55	4.87	3.40	1.48	-.74	-2.89	-4.72	-6.41	-7.79	-8.19	-8.51	-7.19
502	12.90	9.54	8.28	6.39	5.76	5.58	5.41	5.16	4.87	3.80	2.59	.10	-2.51
	5.60	5.82	5.01	3.98	2.04	-.15	-2.29	-4.18	-6.13	-7.88	-8.36	-9.40	-8.08
558	16.60	13.42	11.54	9.01	7.95	7.19	6.75	6.34	5.84	4.76	3.58	1.20	-1.41
	5.36	5.48	4.56	3.67	1.62	-.67	-3.10	-5.15	-7.30	-9.40	-10.36	-11.88	-10.57
614	19.36	16.18	13.71	10.89	9.56	8.18	7.61	7.05	6.56	5.51	4.79	2.41	-.19
	5.17	5.28	4.21	3.40	1.24	-1.11	-3.94	-6.15	-8.60	-10.91	-11.88	-13.39	-12.08
670	22.40	19.22	16.74	12.97	10.87	9.04	7.90	7.19	6.67	5.74	5.02	2.64	.04
	3.98	4.09	3.02	2.18	-.22	-2.74	-5.40	-7.70	-10.31	-12.52	-13.49	-15.00	-13.69
726	22.46	19.27	16.80	13.03	11.80	9.47	8.05	7.10	6.58	5.65	4.93	2.55	-.05
	2.19	2.31	1.23	.40	-2.00	-4.77	-7.70	-10.29	-12.90	-15.11	-16.08	-17.59	-16.28

Table 3

Mean LWR Reseau Displacement Values

SAMPLE:	80	135	190	245	300	355	410	465	520	575	630	685	740
LINE 60	-18.67	-21.13	-22.57	-23.78	-25.63	-27.17	-29.36	-32.65	-35.87	-40.33	-43.77	-46.96	-50.35
	19.02	18.86	15.52	11.59	6.93	3.48	-1.01	-4.07	-7.62	-9.01	-10.20	-10.49	-10.45
115	-18.60	-21.06	-22.50	-23.71	-24.54	-25.86	-27.57	-30.27	-33.19	-37.65	-41.10	-44.29	-47.67
	17.95	17.79	14.45	10.52	5.86	2.82	-1.39	-3.96	-6.98	-8.38	-9.57	-9.85	-9.82
170	-16.63	-19.10	-20.53	-21.95	-22.93	-24.16	-25.91	-28.37	-30.80	-34.66	-38.10	-41.30	-44.68
	18.65	18.49	15.14	11.33	6.79	3.63	-.27	-3.01	-6.19	-7.56	-8.75	-9.04	-9.00
225	-15.05	-17.52	-18.85	-19.88	-21.15	-22.10	-23.69	-25.83	-27.84	-31.41	-34.99	-38.18	-41.56
	17.52	17.36	14.78	11.21	7.16	4.07	.36	-2.16	-5.13	-6.25	-7.53	-7.82	-7.78
280	-12.46	-14.93	-16.18	-17.74	-18.99	-20.17	-21.46	-23.12	-24.74	-28.05	-30.92	-34.05	-37.43
	19.64	17.05	14.66	11.47	7.80	4.65	1.19	-1.42	-4.00	-5.56	-6.71	-6.93	-6.35
335	-9.06	-11.80	-13.11	-14.92	-16.62	-17.81	-19.21	-20.80	-22.73	-25.44	-28.51	-31.44	-34.82
	19.18	17.07	14.90	12.09	8.88	5.96	2.77	-.11	-2.72	-4.38	-5.53	-6.00	-5.41
390	-5.07	-8.26	-9.98	-12.21	-14.12	-15.32	-16.88	-18.45	-20.10	-22.73	-25.31	-28.28	-31.76
	19.00	17.18	15.28	12.66	9.86	6.85	3.86	1.00	-1.59	-3.52	-4.95	-5.40	-4.98
445	-.84	-4.44	-6.58	-9.20	-11.47	-13.16	-14.84	-16.72	-18.14	-20.85	-23.33	-26.02	-28.97
	18.98	17.69	15.77	13.24	10.51	7.43	4.39	1.45	-1.01	-3.35	-5.06	-5.87	-5.83
500	3.91	-.42	-3.14	-6.41	-9.12	-10.99	-12.99	-14.69	-16.05	-18.45	-20.62	-23.65	-26.61
	19.52	18.32	16.33	13.95	11.21	8.12	5.14	2.08	-.42	-3.07	-4.73	-6.12	-6.08
555	8.69	4.37	.73	-3.15	-6.43	-9.03	-11.31	-13.35	-15.13	-17.70	-20.02	-22.42	-25.37
	20.01	18.82	16.43	13.89	10.90	7.59	4.47	1.31	-1.19	-4.32	-6.23	-7.68	-7.64
610	12.17	7.85	3.98	-.51	-4.13	-7.18	-9.86	-12.14	-14.08	-16.58	-19.01	-21.40	-24.36
	20.48	19.28	16.72	14.06	10.83	7.28	4.05	.65	-2.04	-5.43	-7.15	-8.60	-8.56
665	16.09	11.76	7.89	2.63	-1.84	-5.43	-8.83	-11.29	-13.63	-16.18	-18.61	-21.01	-23.96
	19.56	18.36	15.79	13.09	9.57	5.95	2.52	-.91	-3.65	-6.72	-8.44	-9.89	-9.85
720	16.23	11.90	8.03	2.77	.40	-3.75	-7.75	-10.66	-13.44	-16.00	-18.43	-20.82	-23.78
	18.17	16.98	14.41	11.71	8.18	4.12	.76	-3.23	-5.86	-8.93	-10.65	-12.10	-12.06

Table 4

R_1 Constants for SWP Displacement Correction

SAMPLE:	74	130	186	242	298	354	410	466	522	578	634	690	746
LINE													
54	3•48	2•47	2•37	1•57	1•78	•52	-1•85	-4•48	-8•23	-12•94	-16•26	-20•74	-24•28
	15•35	12•27	9•93	6•44	3•25	•34	-2•23	-4•33	-5•79	-6•01	-6•23	-5•17	-5•05
110	3•45	2•44	2•34	1•54	1•31	•19	-1•51	-3•52	-6•57	-11•29	-14•61	-19•08	-22•63
	13•28	10•20	7•86	4•37	1•18	-1•54	-3•93	-6•02	-7•61	-7•83	-8•05	-7•00	-6•87
166	3•27	2•27	2•16	1•22	1•30	•39	-•95	-2•63	-5•39	-9•01	-12•33	-16•81	-20•35
	12•41	9•33	6•99	3•39	•14	-2•20	-4•82	-7•02	-7•94	-8•65	-8•87	-7•81	-7•69
222	2•81	1•80	1•79	1•27	1•23	•55	-•32	-1•50	-3•59	-6•58	-9•70	-14•18	-17•72
	10•89	7•81	5•66	2•32	-•26	-2•73	-4•70	-6•72	-7•97	-8•67	-8•80	-7•75	-7•62
272	3•73	1•78	1•99	1•14	1•21	1•29	•64	•15	-1•53	-3•70	-5•99	-10•21	-13•75
	8•31	6•32	4•56	2•00	-•70	-3•10	-5•32	-6•89	-8•01	-8•66	-9•05	-7•77	-5•79
334	5•48	3•34	3•17	2•26	2•24	2•30	1•81	1•69	•31	-2•11	-4•03	-7•71	-11•25
	6•77	5•53	4•35	2•28	•12	-2•42	-4•46	-6•22	-7•64	-8•52	-8•51	-7•74	-5•76
390	7•11	4•85	4•33	3•23	3•19	3•25	3•11	2•84	2•29	•58	-•93	-4•17	-7•22
	6•05	5•21	4•12	2•47	•46	-1•65	-3•64	-5•44	-6•90	-7•96	-8•28	-7•81	-6•33
446	10•28	7•25	6•47	5•19	4•66	4•54	4•51	4•48	3•58	2•31	•86	-1•68	-4•19
	5•14	4•84	4•35	2•73	•81	-1•43	-3•39	-5•37	-6•78	-8•47	-8•62	-8•93	-7•55
502	12•68	9•35	8•28	6•73	6•12	6•02	6•08	5•69	5•57	4•62	3•45	•79	-1•72
	5•04	5•45	4•55	3•61	1•67	-•51	-2•73	-4•44	-6•53	-8•33	-8•68	-9•87	-8•50
558	16•60	13•28	11•62	9•17	8•21	7•51	7•28	7•07	6•59	5•55	4•35	2•23	-•28
	4•85	5•04	4•22	3•28	1•27	-1•07	-3•32	-5•25	-7•60	-9•54	-10•60	-12•05	-10•67
614	19•36	16•04	13•62	11•01	9•90	8•50	8•21	7•57	7•44	6•40	5•65	3•53	1•01
	4•97	5•16	3•98	3•22	•91	-1•27	-3•98	-6•43	-8•66	-10•90	-12•02	-13•47	-12•09
670	22•43	19•11	16•70	13•06	11•13	9•38	8•32	7•75	7•47	6•59	5•84	3•72	1•20
	3•84	4•03	2•85	2•04	-•20	-2•74	-5•42	-7•76	-10•33	-12•49	-13•62	-15•06	-13•69
726	22•49	19•17	16•76	13•12	12•06	9•84	8•48	7•59	7•31	6•43	5•68	3•56	1•04
	2•00	2•19	1•01	•20	-2•04	-4•62	-7•60	-10•16	-12•74	-14•90	-16•02	-17•46	-16•09

Table 5

R_2 THDA Coefficients for SWP Displacement Correction

SAMPLE:	74	130	186	242	298	354	410	466	522	578	634	690	746
LINE													
54	-.022 .170	-.012 .176	-.024 .164	-.034 .152	-.060 .162	-.066 .159	-.068 .145	-.095 .143	-.073 .114	-.080 .109	-.089 .105	-.104 .112	-.118 .112
110	-.022 .163	-.011 .169	-.024 .156	-.034 .144	-.055 .155	-.042 .145	-.059 .130	-.094 .136	-.095 .139	-.102 .134	-.110 .129	-.125 .137	-.140 .136
166	-.026 .144	-.016 .150	-.028 .138	-.031 .137	-.089 .153	-.058 .119	-.074 .132	-.089 .141	-.068 .102	-.088 .118	-.097 .113	-.112 .121	-.126 .120
222	-.023 .118	-.012 .124	-.015 .125	-.039 .138	-.062 .133	-.044 .112	-.059 .087	-.073 .089	-.090 .098	-.097 .109	-.094 .101	-.109 .108	-.124 .108
272	.004 .119	-.008 .110	-.026 .123	-.030 .101	-.042 .112	-.063 .102	-.058 .120	-.082 .086	-.067 .075	-.115 .084	-.093 .100	-.097 .071	-.111 .068
334	.021 .101	-.009 .108	-.007 .100	-.025 .095	-.037 .087	-.062 .110	-.059 .098	-.100 .098	-.095 .092	-.073 .093	-.090 .074	-.092 .063	-.106 .060
390	.003 .077	-.005 .072	-.007 .082	-.023 .081	-.041 .079	-.047 .067	-.059 .063	-.072 .061	-.086 .064	-.095 .071	-.093 .065	-.115 .051	-.133 .047
446	.029 .063	.008 .080	-.007 .059	-.027 .076	-.038 .075	-.040 .078	-.049 .057	-.080 .073	-.071 .043	-.088 .077	-.083 .050	-.110 .048	-.120 .042
502	.022 .063	.019 .043	-.002 .054	-.040 .042	-.042 .043	-.049 .042	-.075 .050	-.060 .030	-.078 .047	-.092 .052	-.096 .039	-.076 .056	-.086 .050
558	-.001 .058	.013 .051	-.011 .039	-.020 .044	-.030 .041	-.036 .046	-.060 .025	-.083 .013	-.085 .034	-.088 .018	-.085 .028	-.116 .020	-.126 .013
614	.001 .022	.015 .015	.008 .027	-.014 .021	-.039 .038	-.036 .019	-.067 .006	-.059 .033	-.100 .009	-.100 .000	-.096 .018	-.126 .010	-.137 .004
670	-.004 .015	.011 .008	.004 .020	-.011 .018	-.031 -.001	-.039 .001	-.048 .005	-.064 .009	-.090 .006	-.096 -.003	-.092 .015	-.122 .007	-.132 .001
726	-.004 .020	.011 .013	.004 .026	-.011 .023	-.030 .005	-.042 -.016	-.049 -.009	-.055 -.012	-.082 -.016	-.087 -.024	-.083 -.006	-.114 -.014	-.124 -.021

Table 6

Coefficients Defining the Dispersion Relations for the Small Aperture*

	SWP High	SWP Low	LWR High	LWR Low
a_1	981.209	982.251	-5094.526	-298.612
b_1	-6566.373	-263.500	15466.845 (3)	-265.508
a_2	-17760.506(-5)	-466.519(-3)	14925.106(-5)	302.371(-3)
b_2	-12709.243(-5)	376.206(-3)	-27798.582(-5)	225.700(-3)
a_3	12924.643(-10)		-5566.622(-10)	
b_3	12553.362(-10)		9089.256(-10)	
a_4	3.131(-2)		02.18 (-2)	
b_4	0		8.456(-2)	
a_5	-465.499(-3)		275.161(-3)	
b_5	407.922(-3)		223.411(-3)	
a_6	-2.268(-7)		0	
b_6	0.172(-7)		-0.766(-7)	
a_7	-1.440(-8)		11.722(-8)	
b_7	-23.770(-8)		1.770(-8)	
$W_1(s)$	-1.704	-2.033	4.855	4.483
$W_1(l)$	-2.357	-1.536	-8.347	-8.235
$W_2(s)$	0.0352	0.0206	-0.2797	-0.2165
$W_2(l)$	0.2262	0.1761	0.5522	0.5035
$W_3(s)$	1.841(-3)	2.435(-3)	-1.556(-3)	-2.172(-3)
$W_3(l)$	0.658(-3)	0.138(-3)	1.482(-3)	2.204(-3)
Plate Scale	7.72 km s^{-1} px^{-1}	1.67 Å px^{-1}	7.27 km s^{-1} px^{-1}	2.65 Å px^{-1}

The values listed should be multiplied by the power of 10 given in parentheses. The values are to an accuracy such that the contribution of each term can be computed to ∿0.001 pixel in the range of interest.

*See the end of Section V regarding the large aperture.

REFERENCES

Boggess, A. et al.: 1978, Nature 275, 377.

Harvel, C.A., Turnrose, B.E. and Bohlin, R.C.,: 1979, "IUE Data Reduction III. Accuracy of Low Dispersion Wavelengths," NASA IUE NEWSLETTER No. 5.

Klinglesmith, D.A., Perry, P.M., and Turnrose, B.E.: The International Ultraviolet Explorer Spectral Image Processing System. Proceedings of the Society of Photo-Optical Instrumentation Engineers, vol. 172, 1979, p. 279.

Leckrone, D.S.: 1980, "IUE Data Reduction XV. Systematic Errors in the SWP Wavelength Scale," NASA IUE NEWSLETTER No. 10, p. 25.

Oliver, M., Settle, J., Shuttleworth, T., and Sandford, M.: 1979, Report to the 3-Agency Committee on IUE Image Processing, IUE Technical Note No. 44, Appleton Laboratory, University College London.

Thompson, R.W., Turnrose, B.E., and Bohlin, R.C.: 1980, "Effects of Temperature Fluctuations on IUE Data Quality", in The Universe at Ultraviolet Wavelengths: The First Two Years of IUE. ed. R.D. Chapman (NASA CP 2171), p. 811.

Thompson, R.W., Turnrose, B.E., Harvel, C.A., and Bohlin, R.C.: 1980a, in IUE Data Reduction, ed. W.W. Weiss, et al. (Vienna: Austrian Solar and Space Agency), p. 93.

Thompson, R.W., Bohlin, R.C., Turnrose, B.E., and Harvel, C.A.: 1980b, "IUE Data Reduction XVII. Mean Reseaux and Dispersion Constants." NASA IUE NEWSLETTER No. 11, p. 10.

Turnrose, B.E., Bohlin, R.C., Holm, A.V., and Harvel, C.A.: 1979, "IUE Data Reduction V. Wavelength Assignments for Large Aperture Spectra," NASA IUE NEWSLETTER No. 6, p. 180.

Turnrose, B.E., Bohlin, R.C., and Lindler, D.J.: 1981, "IUE Data Reduction XVIII. Implementation of New Low Dispersion Software: Summary of Output Format Changes," NASA IUE NEWSLETTER No. 12, p.2.

Turnrose, B.E., and Bohlin, R.C.: 1981, "IUE Data Recution XX. High Dispersion Line Libraries," NASA IUE NEWSLETTER No. 13.

FIGURE CAPTIONS

Fig. 1(a) - Reseau positions for the SWP camera UVFLOOD images at 3 different head amplifier temperatures. Diamond symbols are plotted at positions of reseaux for the lowest temperature (5.5 C). The lines are vectors representing the displacement of reseaux for the second and third temperatures (9.2 C and 14.2 C), relative to the first temperature. The magnified displacement scale is shown.

(b) - Same as above for the LWR camera and THDA = 10.8, 12.8, and 16.9 C.

Fig. 2 - Gross (upper curve) and background spectra (lowest curve) of HD36981, order 110 SWP 13815, using temperature corrected reseau and dispersion constants. The dashed curve is the background found using mean reseau and dispersion constants. The two gross spectra differ little except for a small shift in the assigned wavelengths.

Fig. 3 - Relative shift of the position in the line and the sample directions for the reseau in row 3, column 7 of SWP. Linear least-squares regression curves are drawn as the solid straight lines, and the equations are written on the figure. The raw scatter of the points about zero and the residual scatter about the fit are also given.

Fig. 4(a) - Scatter in the two orthogonal directions for the reseau locations as observed on 18 SWP flat-field images. The length of the bars represent $\pm$ 1σ scatter.

(b) - Same as above after applying the temperature corrections.

Fig. 5 - Same as Fig. 4 for the LWR camera and 15 flat field images.

Fig. 6 - Spectral format shifts along the dispersion versus THDA. The linear least square regression curves are shown. These high dispersion cases are at 1377.25 Å in order 100 for SWP and 2311.5 Å in order 100 for LWR.

Fig. 7 - Spectral format shifts along the dispersion versus the time of data acquisition for the cameras and wavelengths used for Figure 6, after correcting for the shift predicted by the regression lines shown in Figure 6. An obvious secular dependence remains.

Fig. 8 - Scatter for SWP along and perpendicular to the dispersion for each entry in the high dispersion Pt-Ne line library before correction (upper) and after correction (lower) for the correlation with time and THDA. A scatter of 1 pixel and the corresponding velocity along the dispersion is indicated. The data cover the time period from day 91 in 1979 to day 32 in 1981.

Fig. 9 - Same as for Fig. 8 for LWR camera.

Fig. 10 - Same as for Fig. 8 in low dispersion.

Fig. 11 - Same as for Fig. 8 for LWR in low dispersion.

Fig. 12 - Predicted location of the SWP small aperture wavelength 1377.25 Å in high dispersion order 100 for various times and THDA temperatures. The cross (x) at s = 392.41 and l = 258.22 marks the mean position found for the time period from day 91 in 1979 to day 32 in 1981. The direction of increasing wavelength is indicated at the angle of 52° with respect to the sample direction.

Fig. 13 - Same as Figure 12 for SWP low dispersion at 1500 Å. The cross at s = 282.47 and l = 300.81 and the angle of the dispersion direction with respect to the sample direction is 141°.

Fig. 14 - Same as Fig. 12 for LWR high dispersion at 2311.5 Å and order 100. The cross is at s = 361.10 and 1 = 307.16 and the angle is 126°.

Fig. 15 - Same as Fig. 12 for LWR low dispersion at 2600 Å. The cross is at s = 487.55 and 1 = 321.31 and the angle is 37°.

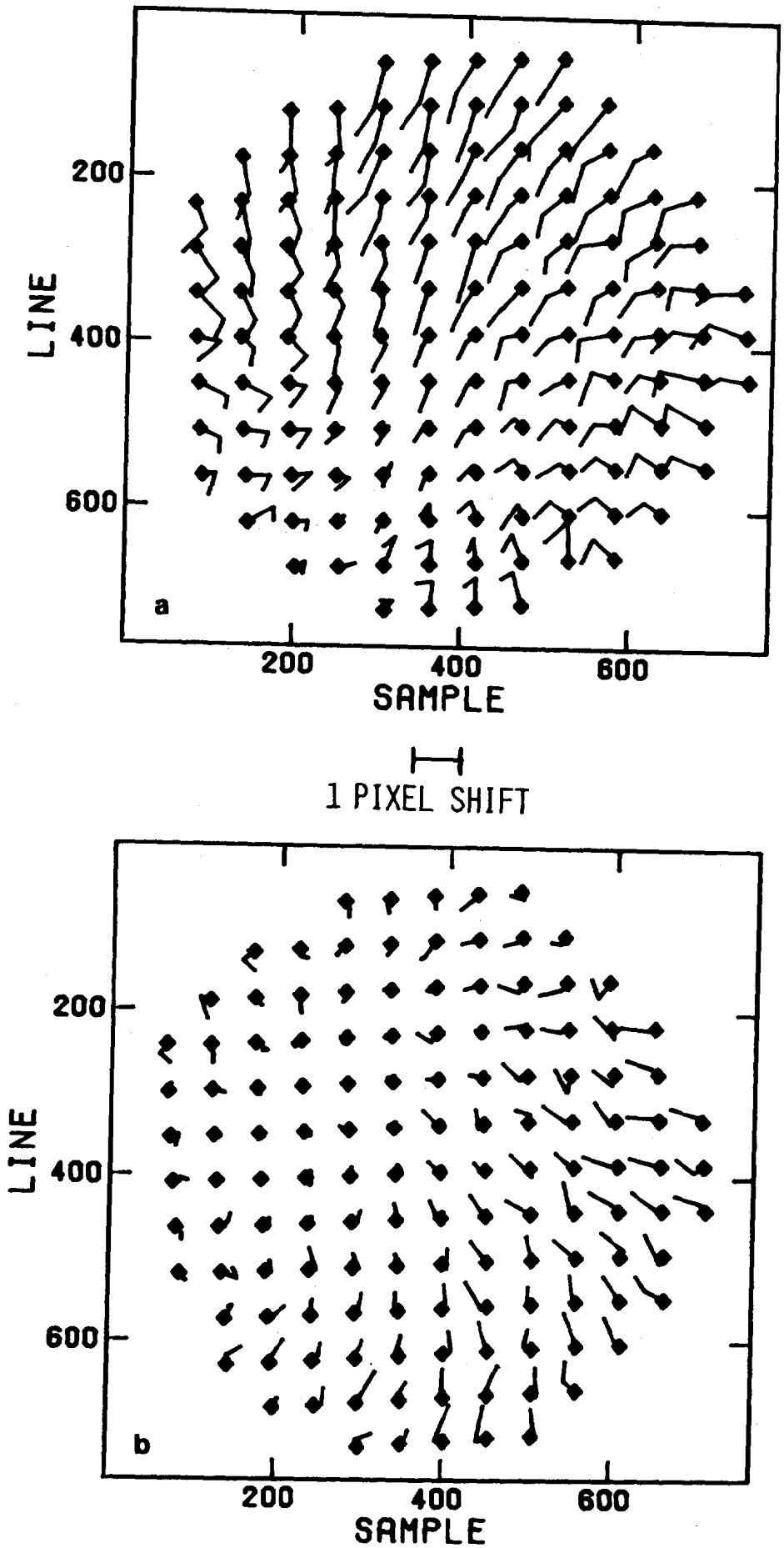
200
400
600
LINE
a
200
400
600
SAMPLE
1 PIXEL SHIFT
200
400
600
LINE
b
200
400
600
SAMPLE

FIGURE 1

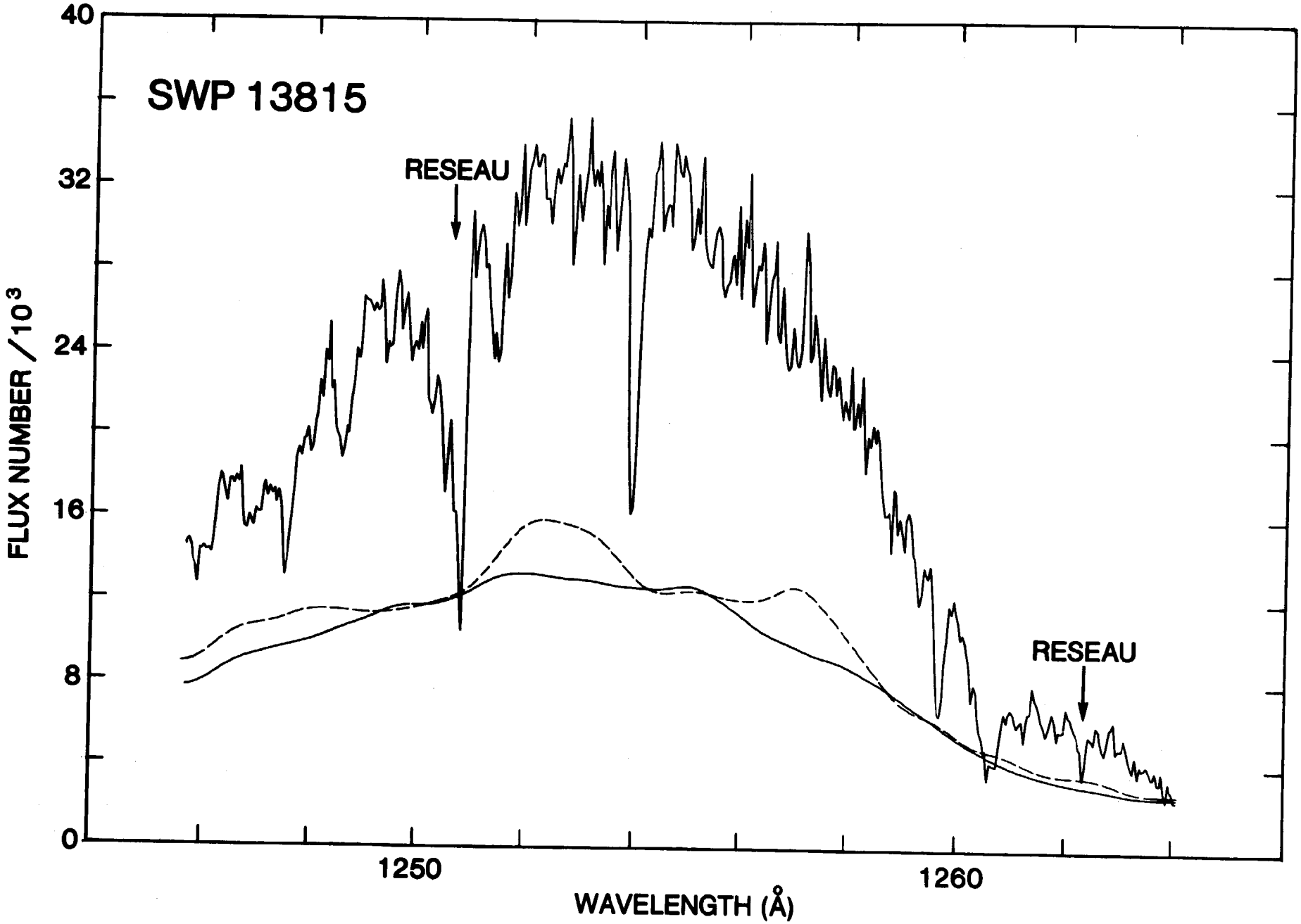
SWP 13815
RESEAU
RESEAU
40
32
24
16
8
0
FLUX NUMBER /10³
1250
1260
WAVELENGTH (Å)

FIGURE 2

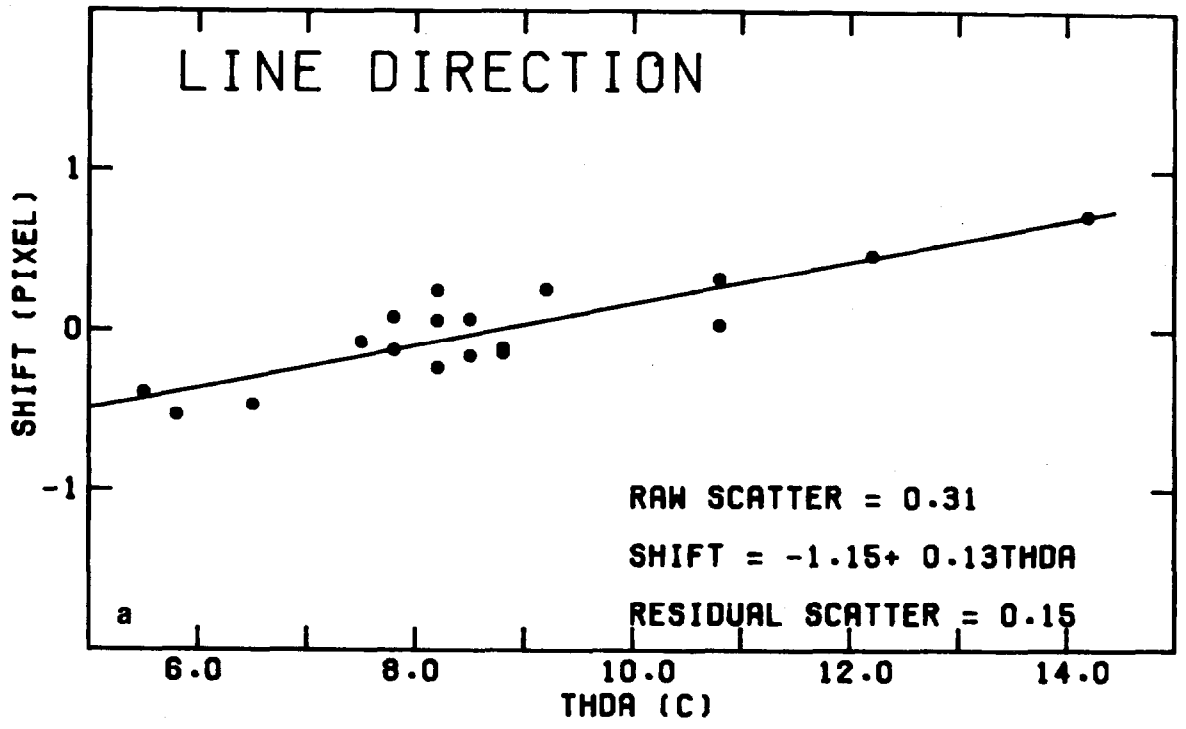
LINE DIRECTION
SHIFT (PIXEL)
1
0
-1
RAW SCATTER = 0.31
SHIFT = -1.15+ 0.13THDA
RESIDUAL SCATTER = 0.15
a
6.0
8.0
10.0
12.0
14.0
THDA (C)

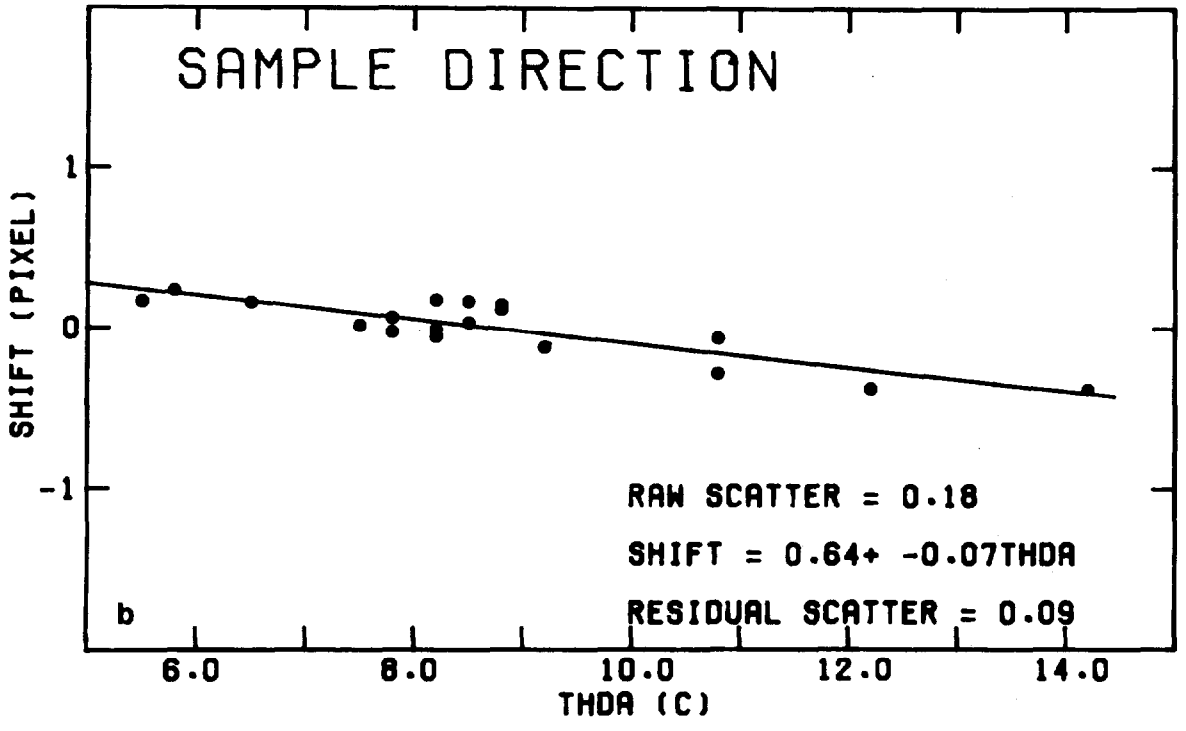
SAMPLE DIRECTION
SHIFT (PIXEL)
1
0
-1
RAW SCATTER = 0.18
SHIFT = 0.64+ -0.07THDA
RESIDUAL SCATTER = 0.09
b
6.0
8.0
10.0
12.0
14.0
THDA (C)

FIGURE 3

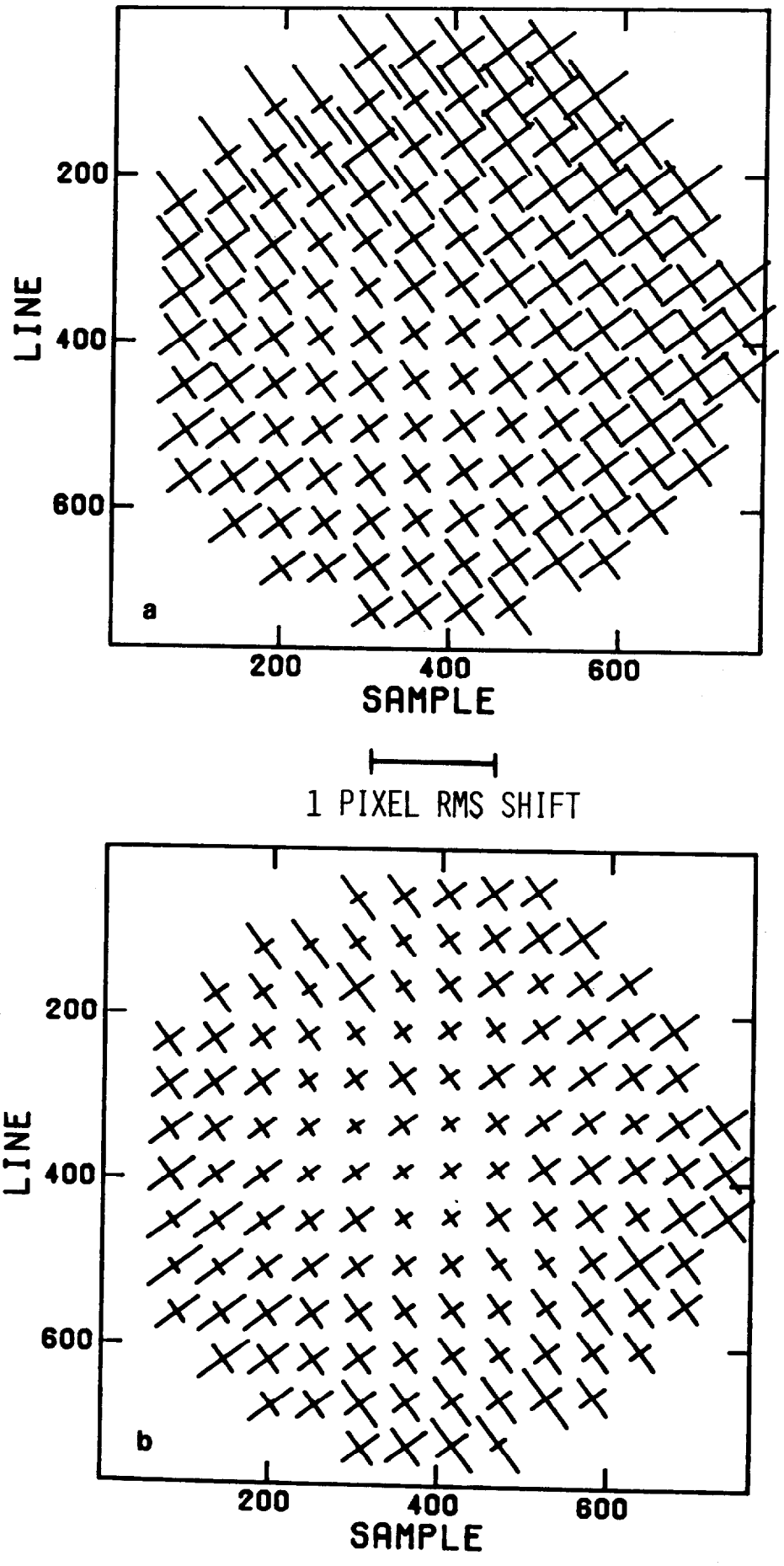
200
400
600
LINE
a
200
400
600
SAMPLE
1 PIXEL RMS SHIFT
200
400
600
LINE
b
200
400
600
SAMPLE

FIGURE 4

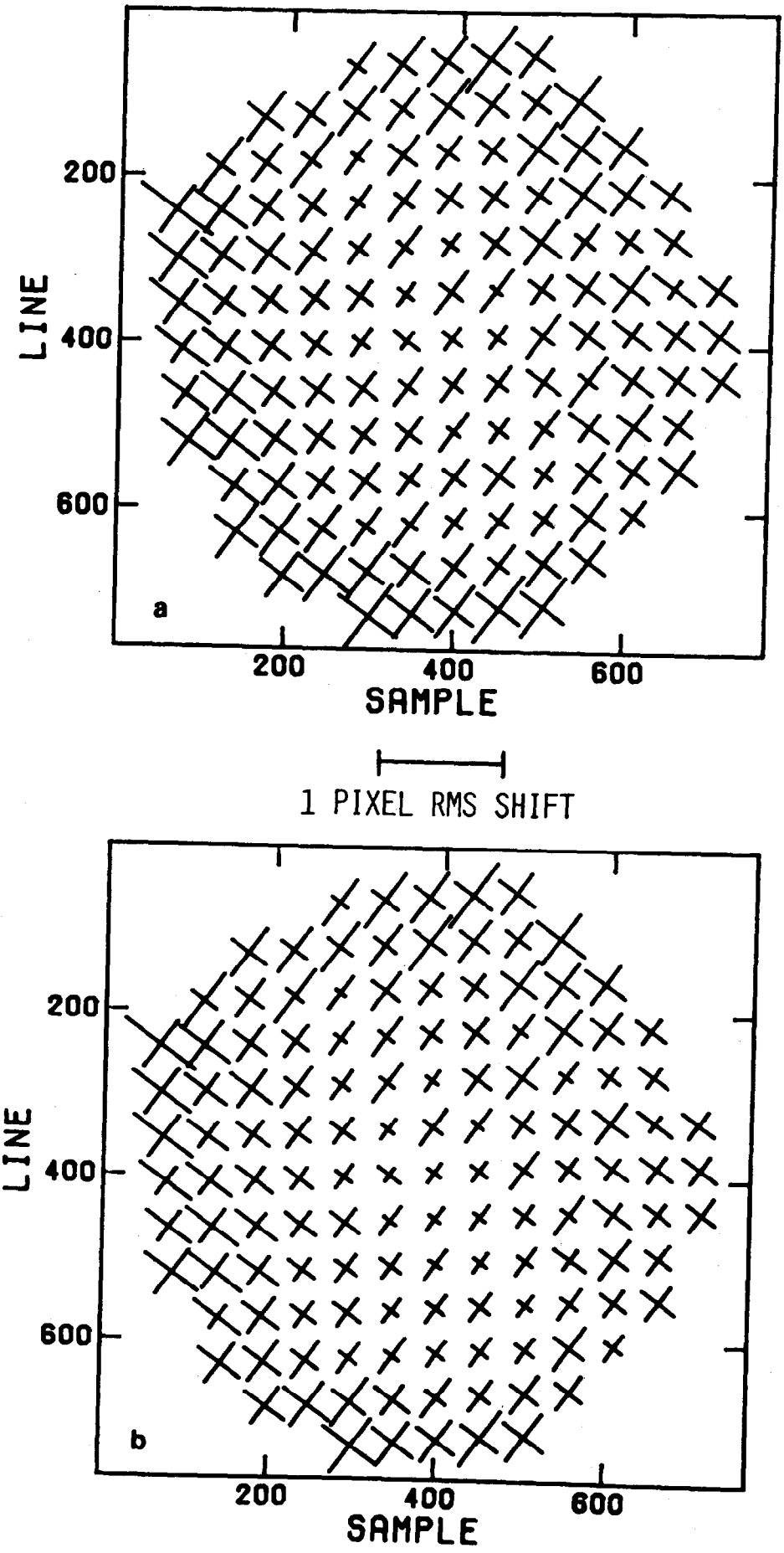
200
400
600
LINE
a
200
400
600
SAMPLE
1 PIXEL RMS SHIFT
200
400
600
LINE
b
200
400
600
SAMPLE

FIGURE 5

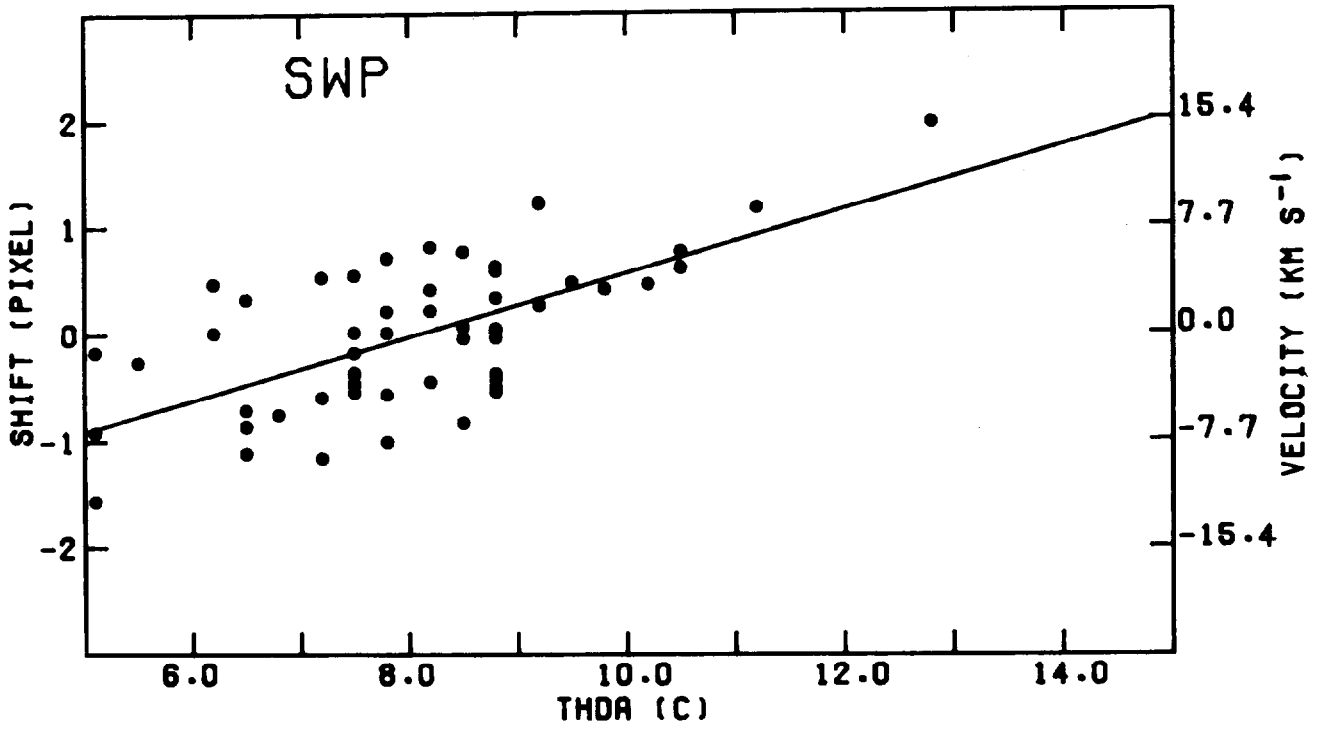
SWP
SHIFT (PIXEL)
2
1
0
-1
-2
15.4
7.7
0.0
-7.7
-15.4
VELOCITY (KM S^{-1})
6.0
8.0
10.0
12.0
14.0
THDA (C)

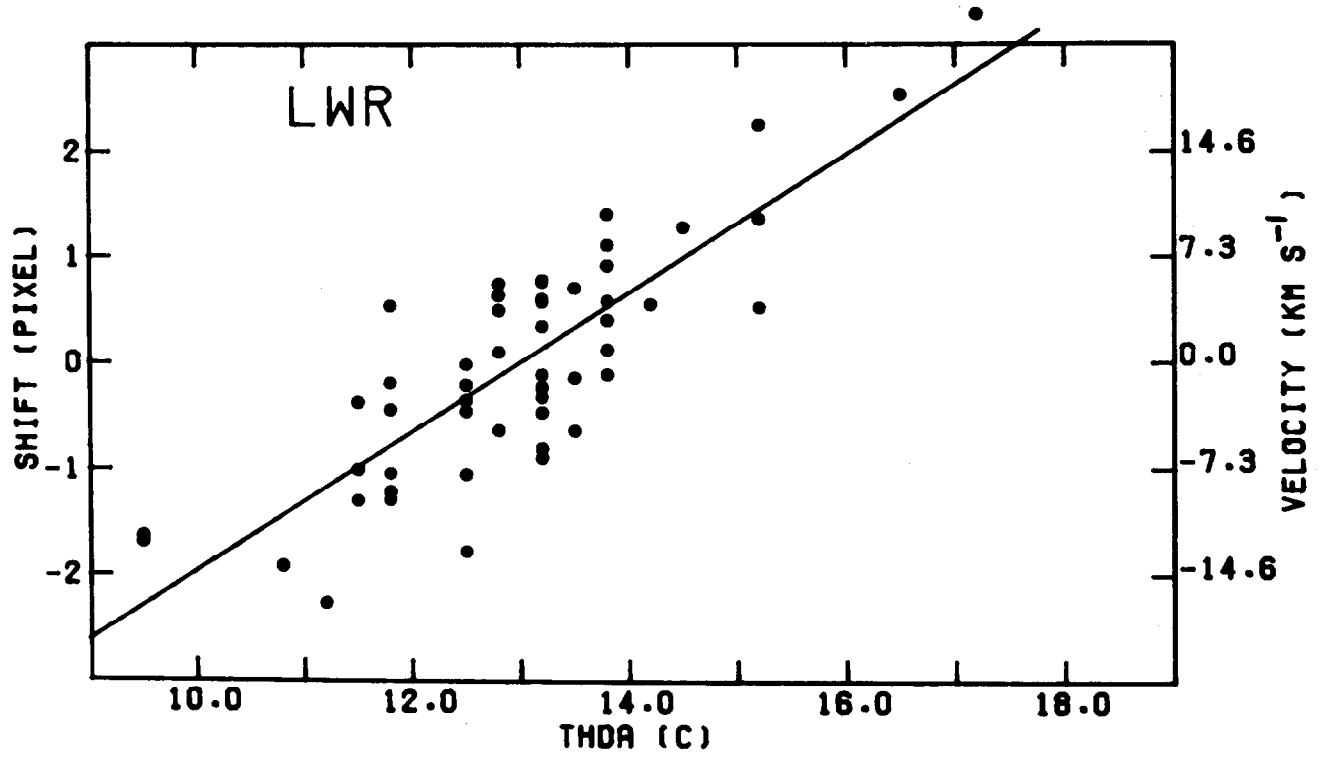
LWR
SHIFT (PIXEL)
2
1
0
-1
-2
14.6
7.3
0.0
-7.3
-14.6
VELOCITY (KM S^{-1})
10.0
12.0
14.0
16.0
18.0
THDA (C)

FIGURE 6

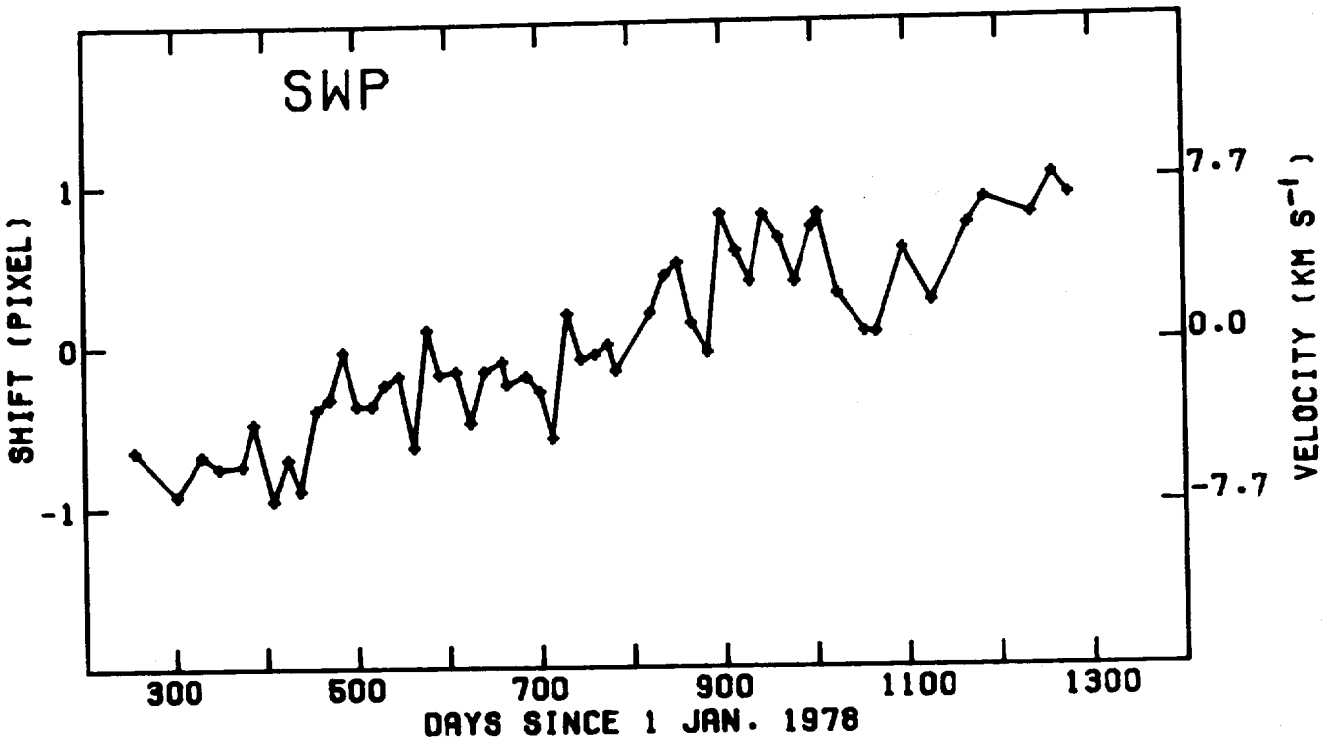
SWP
SHIFT (PIXEL)
1
0
-1
7.7
0.0
-7.7
VELOCITY (KM S^{-1})
300
500
700
900
1100
1300
DAYS SINCE 1 JAN. 1978

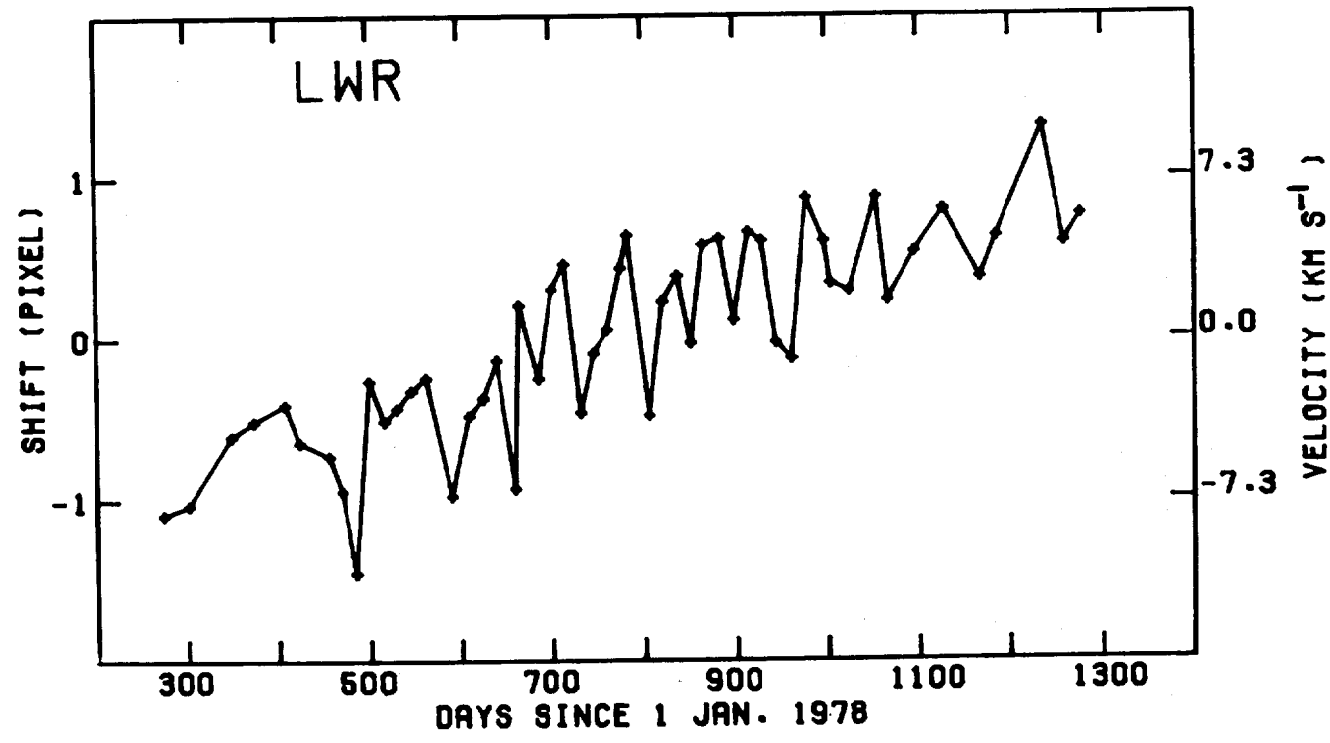
LWR
SHIFT (PIXEL)
1
0
-1
7.3
0.0
-7.3
VELOCITY (KM S^{-1})
300
500
700
900
1100
1300
DAYS SINCE 1 JAN. 1978

FIGURE 7

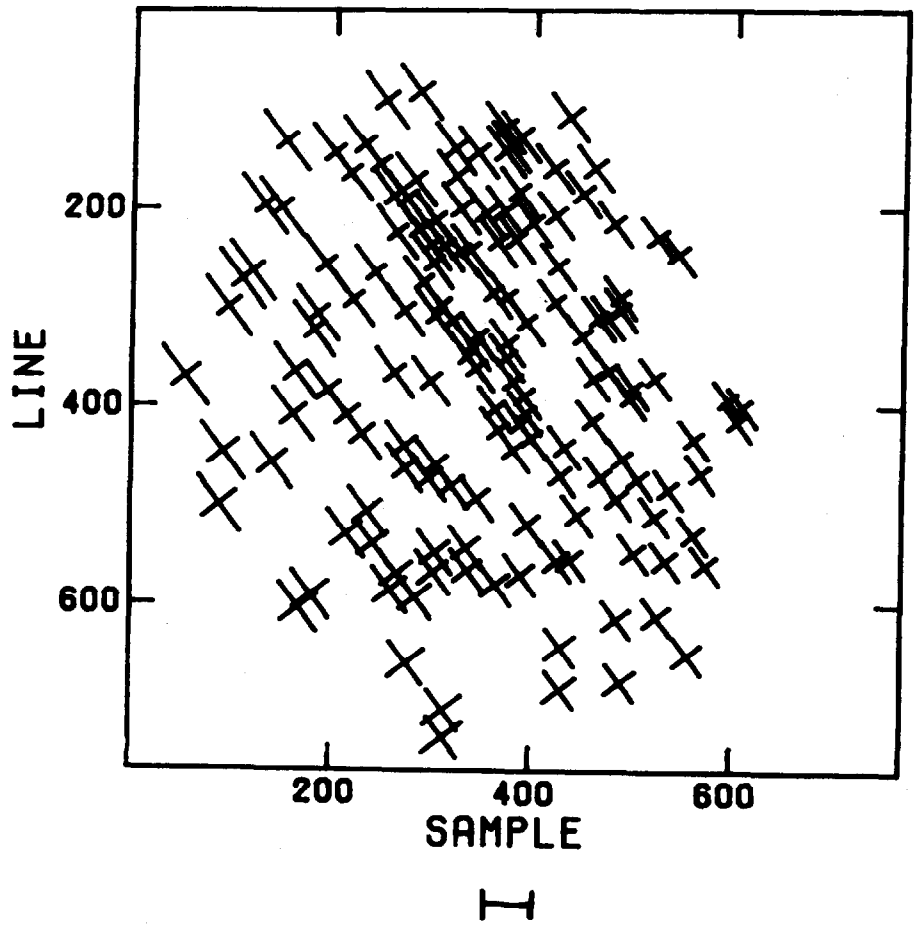

1 PIXEL SHIFT (7.7 KM S^{-1})

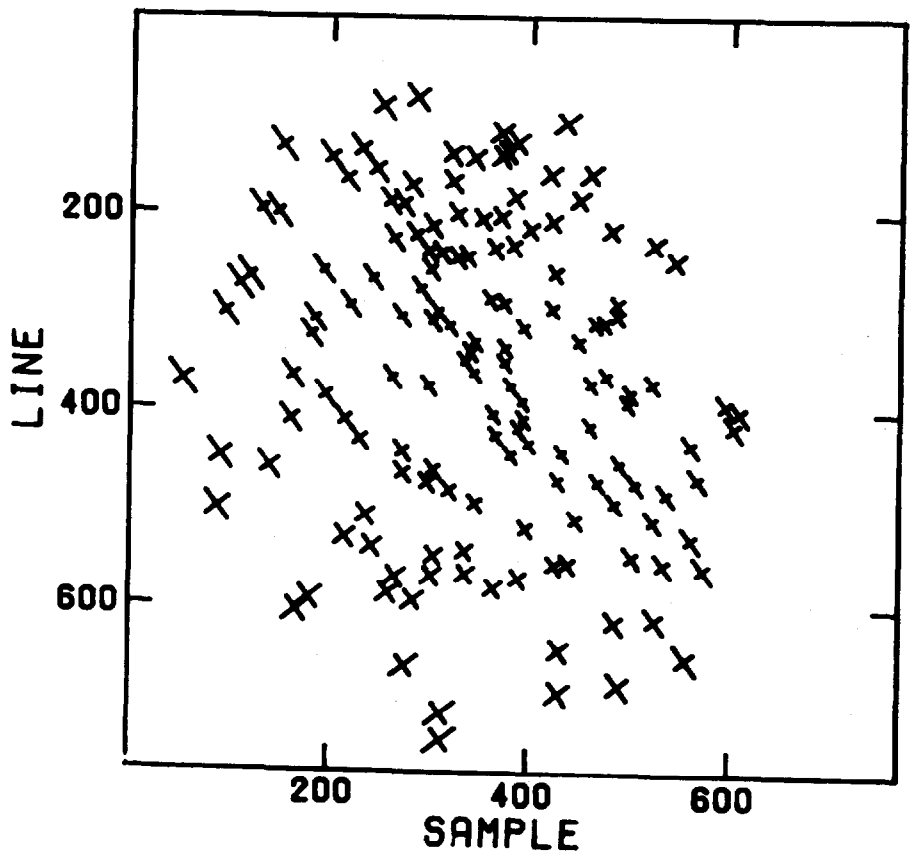

FIGURE 8

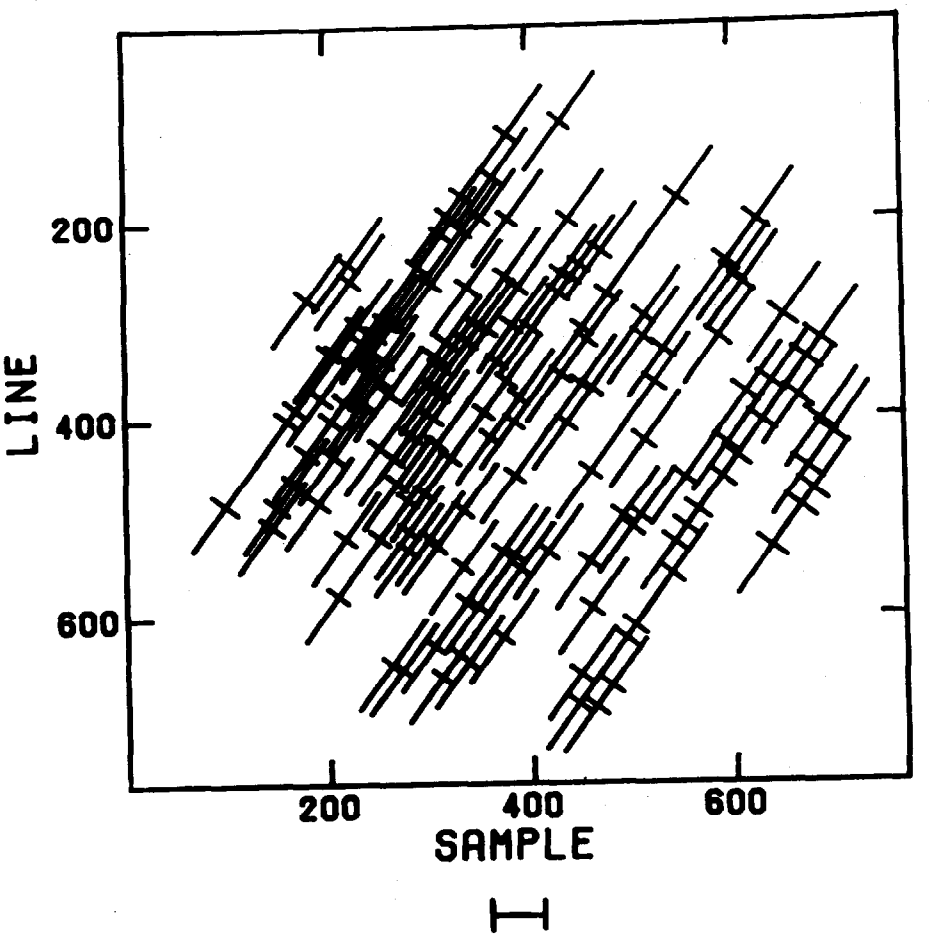

1 PIXEL SHIFT (7.3 KM S^{-1})

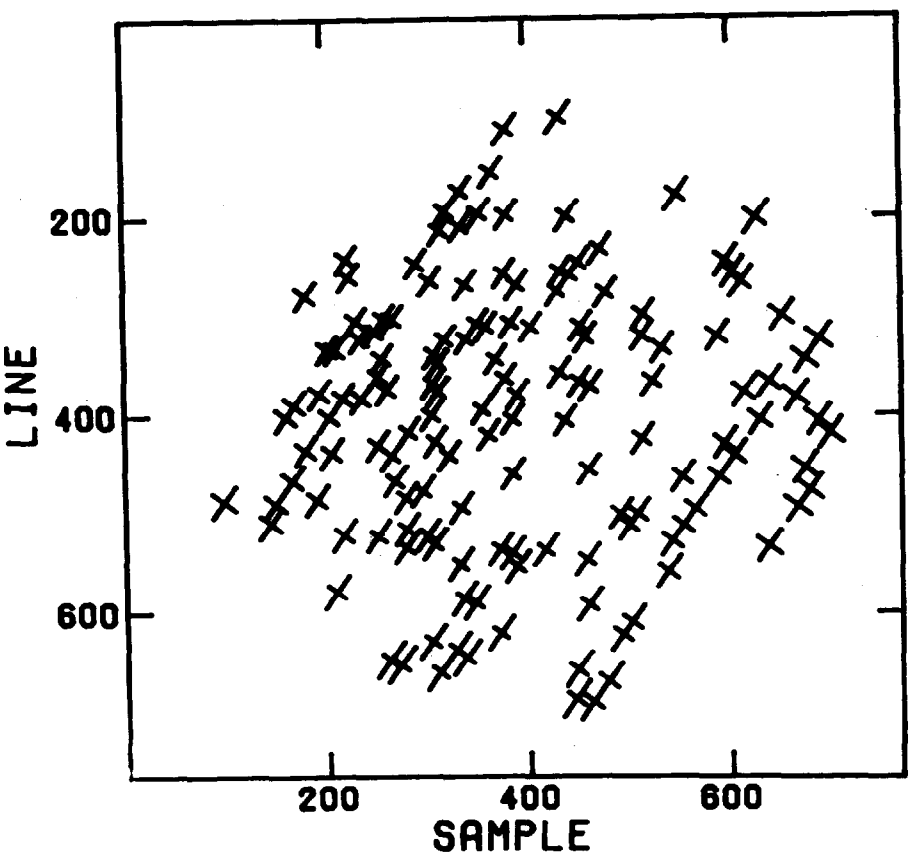

FIGURE 9

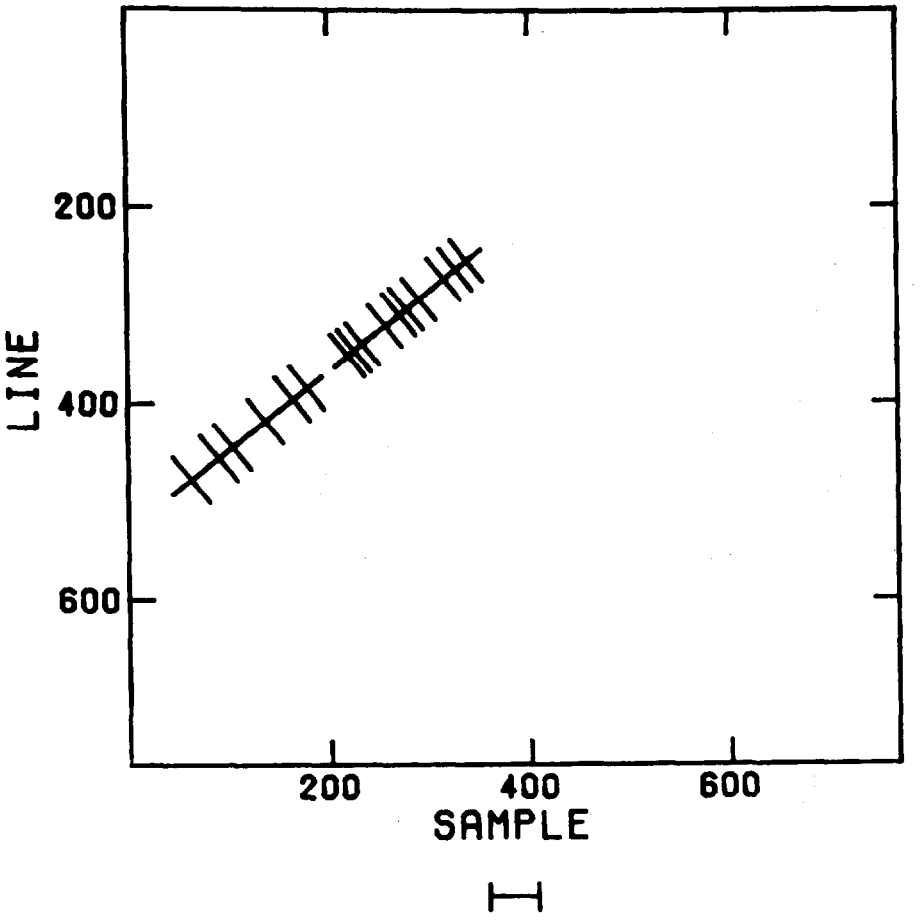

1 PIXEL SHIFT (1.67 Å)

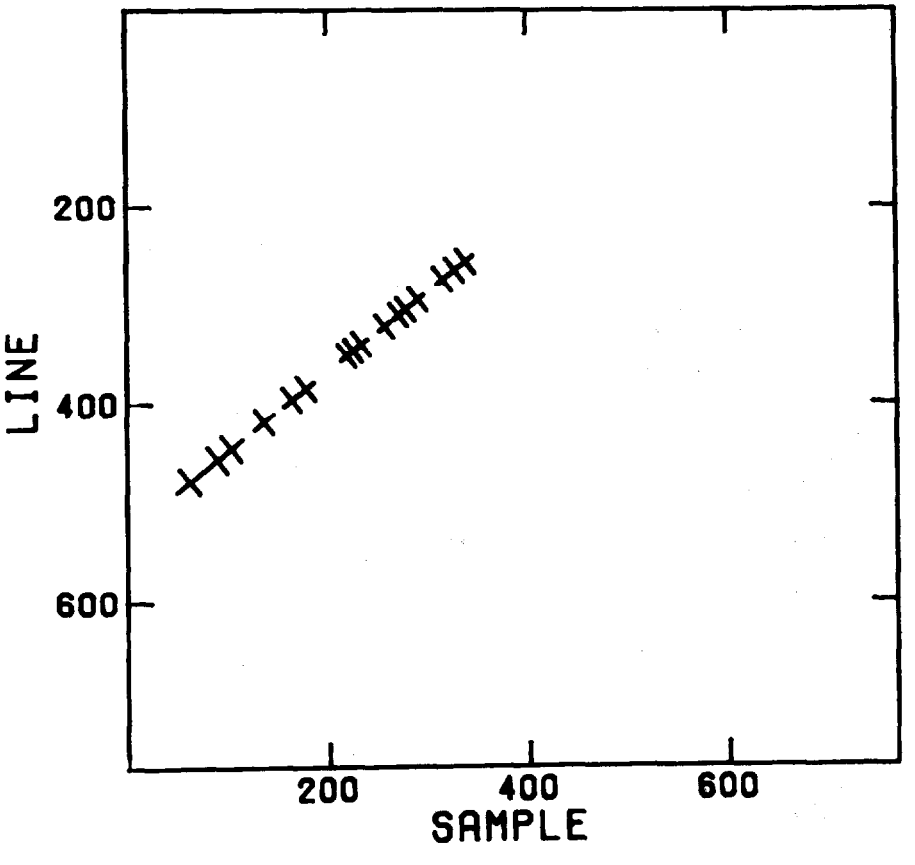

FIGURE 10

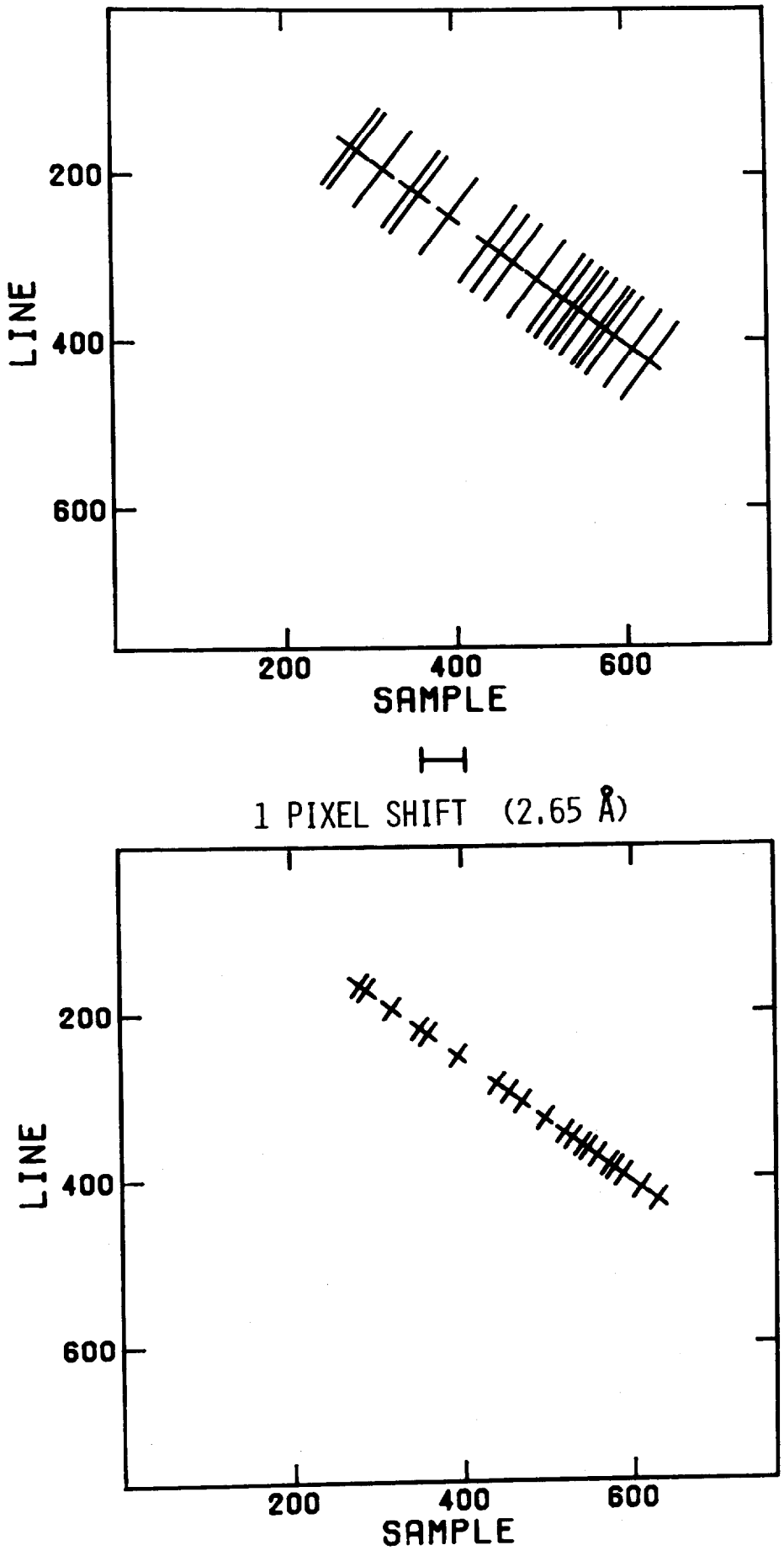
200
400
600
LINE
200
400
600
SAMPLE
1 PIXEL SHIFT (2.65 Å)
200
400
600
LINE
200
400
600
SAMPLE

FIGURE 11

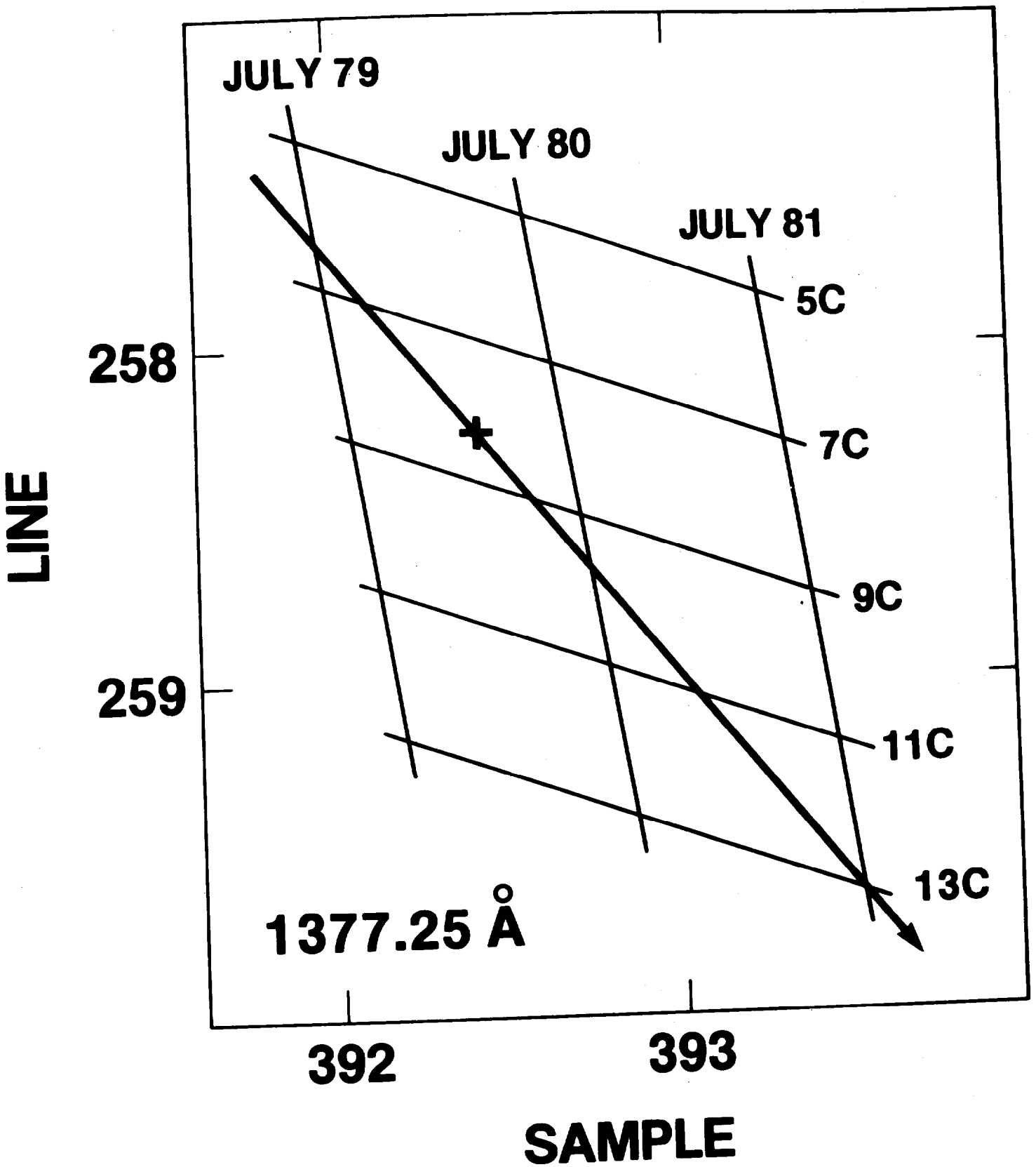
JULY 79
JULY 80
JULY 81
5C
7C
9C
11C
13C
258
259
LINE
1377.25 Å
392
393
SAMPLE

FIGURE 12

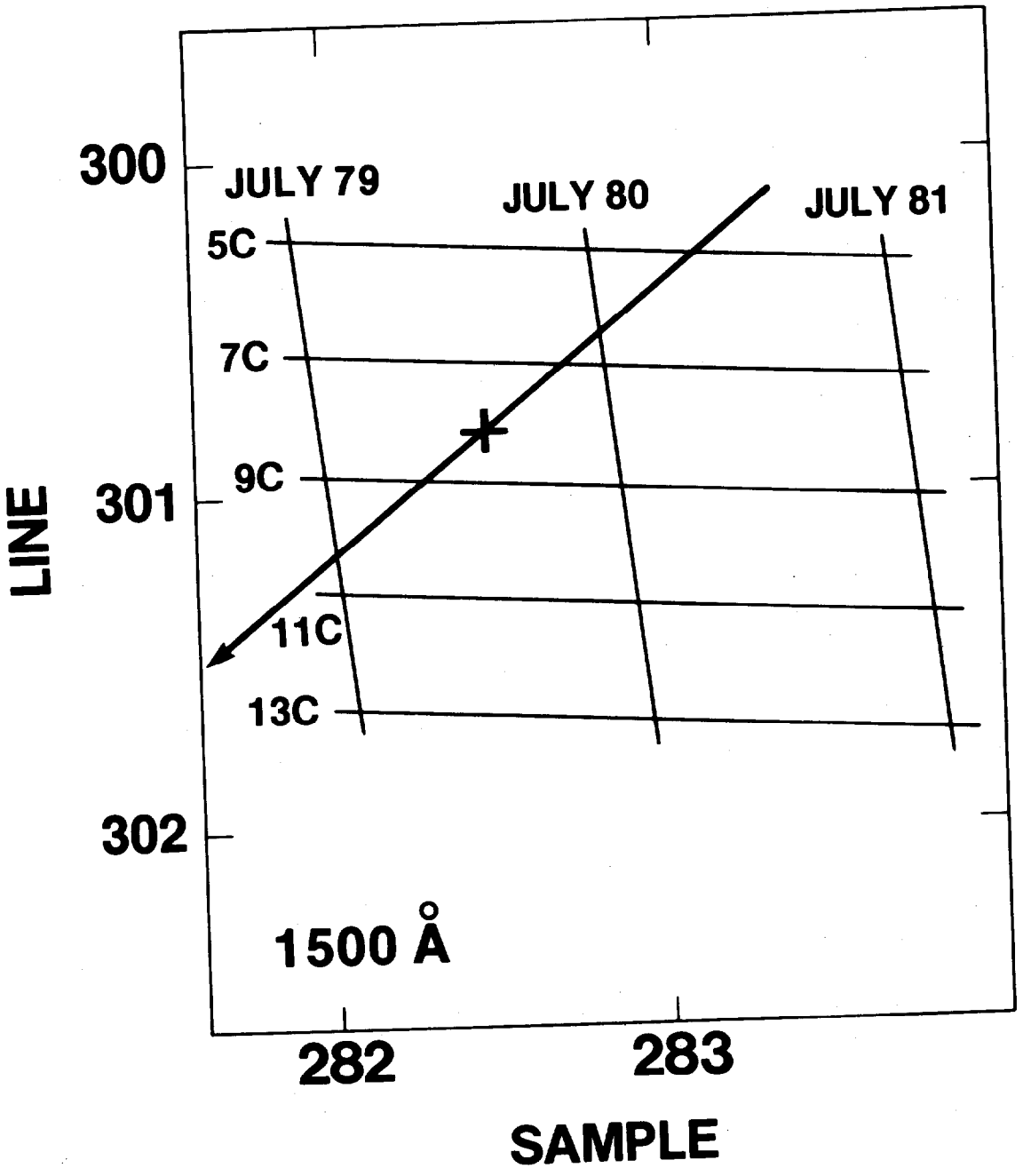
300
301
302
LINE
JULY 79
JULY 80
JULY 81
5C
7C
9C
11C
13C
1500 Å
282
283
SAMPLE

FIGURE 13

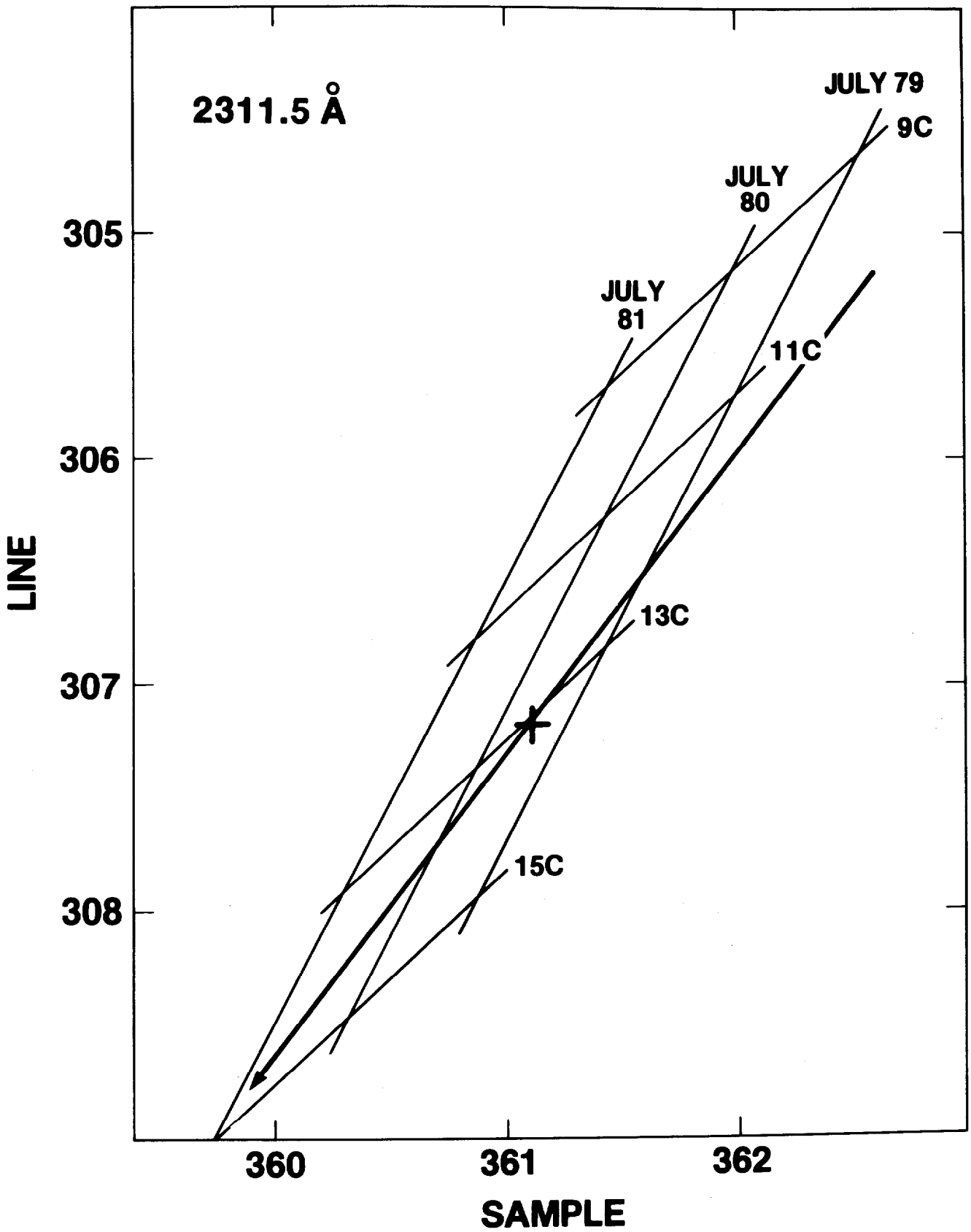
2311.5 Å
JULY 79
9C
JULY
80
JULY
81
11C
13C
15C
305
306
307
308
LINE
360
361
362
SAMPLE

FIGURE 14

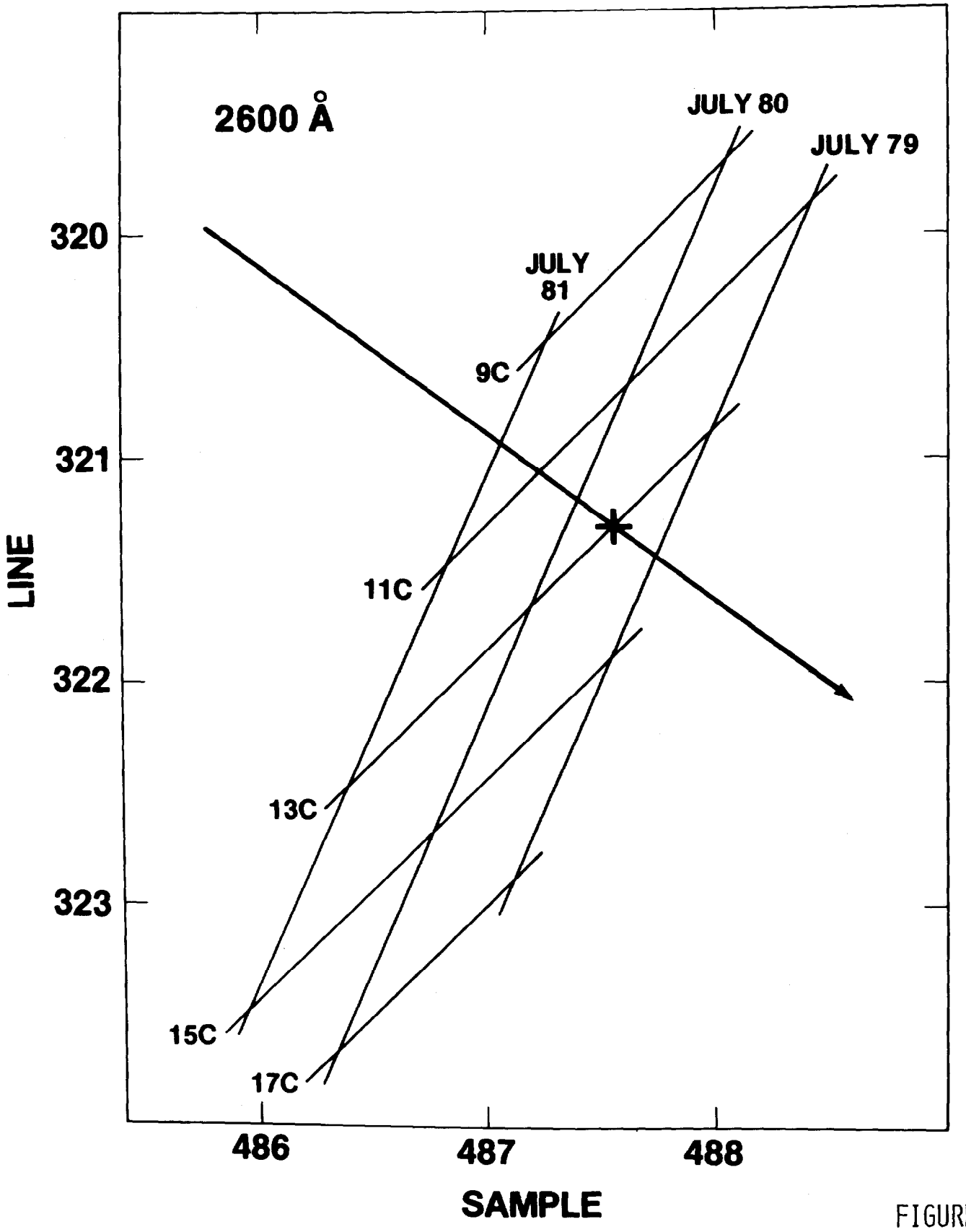
2600 Å
JULY 80
JULY 79
JULY
81
9C
11C
13C
15C
17C
320
321
322
323
LINE
486
487
488
SAMPLE

(52)

FIGURE 15